

Isospin-Violating Dark Matter at the LHC

Kaoru Hagiwara^a, Danny Marfatia^b, Toshifumi Yamada^{a,c}

^a *KEK Theory Center and SOKENDAI,
1-1 Oho, Tsukuba, Ibaraki 305-0801, Japan*

^b *Department of Physics & Astronomy, University of Hawaii, Honolulu, HI 96822, U.S.A
and*

Department of Physics & Astronomy, University of Kansas, Lawrence, KS 66045, USA

^c *Department of Physics, University of Tokyo,
7-3-1 Hongo, Bunkyo-ku, Tokyo 113-0033, Japan*

Abstract

We consider a toy model of dark matter (DM) with a gauge singlet Dirac fermion that has contact interactions to quarks that differ for right-handed up and down quarks. This is motivated by the isospin-violating dark matter scenario that was proposed to reconcile reported hints of direct DM detection with bounds from non-observation of the signal in other experiments. We discuss how the effects of isospin violation in these couplings can be observed at the LHC. By studying events with large missing transverse momentum (\cancel{E}_T), we show that the ratio of mono-photon and mono-jet events is sensitive to the ratio of the absolute values of the couplings to the up and down quarks, while a dedicated study of di-jet plus \cancel{E}_T events can reveal their relative sign. We also consider how our results are modified if instead of a contact interaction, a particle that mediates the interaction is introduced. Our methods have broad applicability to new physics that involves unequal couplings to up and down quarks.

1 Introduction

Once a hint of dark matter (DM) is found in events with large missing transverse momentum (\cancel{E}_T) at the LHC, the next task will be to study how the DM particle couples to standard model (SM) particles. It can be the case that the DM particle couples to up and down quarks differently. Observing such an isospin violating feature of the new physics sector would give an important clue for the determination of the Lagrangian of the underlying theory. Also, it is itself a challenge in the physics of hadron colliders, requiring elaborate kinematical cuts to extract information from parton-level processes.

In this context, isospin-violating dark matter (IVDM) [1] provides a scenario in which a DM particle does not couple identically to up and down quarks. This model was motivated by DM direct detection experiments. The DAMA [2] and CoGeNT [3] experiments observed signals that are potentially of dark matter origin. The signals are consistent with a DM particle of mass 10 GeV scattering off nuclei with a spin-independent nucleon cross section of $\sigma_N \sim 2 \times 10^{-4}$ pb and $\sigma_N \sim 7 \times 10^{-5}$ pb, respectively. However, the XENON [4] and CDMS [5] experiments reported negative results. To accommodate the apparently inconsistent data, the authors of Ref. [1] considered a dark matter particle that couples to up and down quarks differently. Then the cross section of dark matter scattering off protons differs from that off neutrons, and the apparent tension among dark matter direct detection experiments is attributed to the different proton-neutron ratios of the detector materials. Recently, the LUX experiment [6] has reported a stringent upper bound on the spin-independent cross section for DM elastic scattering off nuclei. A tension between the LUX and the DAMA/CoGeNT results persists even if isospin-violating couplings of DM are assumed [7], because liquid xenon is composed of several isotopes so that it is not possible to completely suppress xenon's coupling to DM [1]. More recently, the SuperCDMS [8] and CDEX [9] experiments have also reported null results that corroborate the LUX results. Nevertheless, independently of the aforementioned anomalies in the context of light DM, the possibility that a generic DM particle interacts with SM quarks through isospin-violating couplings remains and should be investigated.

We study the possibility of testing the scenario at the LHC by measuring the couplings to up and down quarks. We work in a general context and simply assume that a new stable particle that is a singlet under the SM gauge group (called “dark matter” in the following) couples to right-handed up and down quarks with different strengths and signs. At the LHC, the production of DM particles associated with a jet(s) or photon gives rise to events with a hard jet(s) or photon plus large missing transverse momentum (\cancel{E}_T). Since the up and down quarks couple differently to the photon but identically to the gluons, the magnitudes of the two couplings can be measured by comparing the cross section of the mono-jet plus \cancel{E}_T signal

with that of the mono-photon plus \cancel{E}_T signal. The relative sign of the dark matter couplings is more difficult to measure because it requires the measurement of the interference between the dark matter coupling to the up quark and that to the down quark. This is possible through the subprocess, $ud \rightarrow ud + DM DM$, but the interference effects need to be identified in the presence of the other dijet+ $DM DM$ subprocesses and the SM backgrounds.

Our discussion of how isospin-violating couplings of a DM particle can be studied at the LHC involves several ingredients. We use MadGraph 5 [10] for calculating matrix elements and for generating DM signal events, Pythia 8 [11] for parton showering, and PGS 4 [12] for simulating detector effects. The outline of the paper is as follows. In Section 2, we describe our toy model of IVDM. In Sections 3, 4 and 5, we investigate the DM signals from three channels, mono-jet plus \cancel{E}_T , mono-photon plus \cancel{E}_T , and di-jet plus \cancel{E}_T . In Section 6, we present the latest LHC bounds on the contact interaction scale for couplings that suppress scattering in xenon detectors. In Section 7, we consider a model in which isospin-violating interactions result from a mediator field that couples to the DM and quarks, and study how the presence of the mediator enhances the DM signal cross sections. Section 8 is devoted to discussion and conclusion.

2 Model

We consider a toy model in which a DM particle couples to quarks with isospin-violating couplings. We introduce a Dirac fermion χ that is a singlet under the SM gauge group. It couples to the up and down quarks through vector-like and axial vector-like contact interactions. The relevant part of the Lagrangian is

$$\mathcal{L}_{DM} = i\bar{\chi}\gamma^\mu\partial_\mu\chi - m_\chi\bar{\chi}\chi + \frac{1}{\Lambda^2}(g_Q\bar{q}_L\gamma_\mu q_L + g_U\bar{u}_R\gamma_\mu u_R + g_D\bar{d}_R\gamma_\mu d_R)(\bar{\chi}\gamma^\mu\chi), \quad (1)$$

where Λ denotes the energy scale of the contact interaction and q_L denotes the SU(2) doublet of left-handed up and down quarks. For $g_U \neq g_D$, χ is IVDM.

At the LHC, we would like to extract the magnitudes and relative signs of the couplings, g_U , g_D and g_Q . In the following, we examine the possibility of measuring g_U/g_D by setting $g_Q = 0$. Implications of $g_Q \neq 0$ will be discussed in the last section.

The (absolute) perturbative unitarity bounds for the DM production processes $u_R\bar{u}_R \rightarrow \chi\bar{\chi}$ and $d_R\bar{d}_R \rightarrow \chi\bar{\chi}$ are saturated when the center-of-mass energy, s , satisfies

$$\sqrt{s} = (48\pi^2)^{1/4} \frac{\Lambda}{\sqrt{g_q}} \quad (q = u, d). \quad (2)$$

For example, for $\Lambda = 800$ GeV and $g_q = 1$, the perturbative unitarity bound is violated for $\sqrt{s} > 3.7$ TeV. Throughout, we simply assume the cross section for a DM production process to be constant for $\sqrt{s} \geq (48\pi^2)^{1/4} \Lambda/\sqrt{g_q}$, although it will turn out that the results of our analysis are insensitive to the behavior of DM production cross sections for \sqrt{s} near and above the unitarity bound. A detailed discussion of unitarity bounds for inelastic scattering is provided in the Appendix.

3 Mono-jet + \cancel{E}_T

In this section, we study events with a high p_T mono-jet and large \cancel{E}_T , which is the discovery channel for a DM particle at hadron colliders. We first focus on the case of pp collisions at $\sqrt{s} = 7$ TeV and reproduce the results of Ref. [13]. We then consider $\sqrt{s} = 14$ TeV, the target energy of the LHC. By optimizing the selection cuts, we estimate the DM signal for various values of g_U/g_D for a fixed value of $\sqrt{g_U^2 + g_D^2}$ and $g_Q = 0$.

3.1 Study for $\sqrt{s} = 7$ TeV

Following Ref. [13], we adopt the *veryHighPT* cut of the ATLAS search [14], which yields the most stringent bound on the DM-quark interactions. This cut is described by

- Require $\cancel{E}_T > 300$ GeV.
- Highest p_T jet should satisfy $|\eta_1| < 2.0$ and $p_{T1} > 350$ GeV.
- Event is vetoed if the second hardest jet satisfies $|\eta_2| < 4.5$, and $p_{T2} > 60$ GeV or $\Delta\phi(\vec{p}_{T2}, \vec{\cancel{E}}_T) < 0.5$.
- Event is vetoed if there is another jet that satisfies $|\eta| < 4.5$ and $p_T > 30$ GeV.
- Event is vetoed if there is an electron that satisfies $|\eta_e| < 2.47$ and $p_{Te} > 20$ GeV.
- Event is vetoed if there is a muon that satisfies $|\eta_\mu| < 2.4$ and $p_{T\mu} > 10$ GeV.

The dominant sources of background for mono-jet events that satisfy the above criteria are Z + jet events with $Z \rightarrow \nu\nu$, and W + jet events with $W \rightarrow \tau\nu$ or $W \rightarrow l\nu$ ($l = e, \mu$) where the τ decay products or leptons do not satisfy any of the veto criteria.

We estimate the Z + jet background by first generating $Z(\rightarrow \nu\nu) + 1, 2$ jets events at the matrix element level [10] with precuts $\cancel{E}_T > 200$ GeV and $k_T > 140$ GeV for the jets. We

Background	Our simulation	ATLAS collaboration	Normalization factor
$Z(\nu\nu) + \text{jets}$	106	$124 \pm 12 \pm 15$	1.17
$W(\tau\nu) + \text{jets}$	35.4	$36 \pm 7 \pm 8$	1.08
$W(e/\mu\nu) + \text{jets}$	22.2	$26 \pm 4 \pm 3$	

Table 1: The numbers of background events that pass the *veryHighPT* cut for 1 fb^{-1} LHC (at 7 TeV) according to our simulation (see Eqs. 3-5), compared to the estimates by ATLAS [14]. The last column gives the ratios of the ATLAS estimate to our estimate.

next simulate parton showering [11] by using the k_T -jet matching scheme [15] to match the p_T distribution of the second hardest jet simulated via the parton showering of $Z + 1$ jet events and the distribution calculated from the matrix elements of $Z + 2$ jets events. The matching scale is set at 200 GeV. We have confirmed that the cross section after the final cut does not change significantly when the matching scale is varied by ± 60 GeV around 200 GeV. Finally, we perform a detector simulation [12] and the cross section for $Z(\rightarrow \nu\nu) + \text{jets}$ events that pass the *veryHighPT* cut is found to be

$$\sigma_{Z(\rightarrow \nu\nu)+\text{jets}}(\textit{veryHighPT}) \simeq 106 \text{ fb}. \quad (3)$$

In a similar manner, we generate $W + 1, 2$ jets events in which W decays into $\tau\nu_\tau$ and those in which W decays into $e\nu_e$ or $\mu\nu_\mu$, at the matrix element level with the precuts $p_T^l > 200$ GeV, where p_T^l denotes the transverse momentum for the three-momentum sum of the lepton momenta, and $k_T > 140$ GeV for the jets. We then simulate parton showering with a matching scale of 200 GeV, and study the detector effects. Again, we have confirmed that the cross section after the final cut does not change much when the matching scale is varied around 200 GeV by ± 60 GeV. The cross sections for $W(\rightarrow \tau\nu_\tau) + \text{jets}$ events and $W(\rightarrow e\nu_e/\mu\nu_\mu) + \text{jets}$ events that pass the *veryHighPT* cut are found to be

$$\sigma_{W(\rightarrow \tau\nu_\tau)+\text{jets}}(\textit{veryHighPT}) \simeq 35.4 \text{ fb}, \quad (4)$$

$$\sigma_{W(\rightarrow e\nu_e/\mu\nu_\mu)+\text{jets}}(\textit{veryHighPT}) \simeq 22.2 \text{ fb}. \quad (5)$$

In Table 1, we compare the numbers of background events estimated in Eqs. (3-5) with those estimated by the ATLAS collaboration [14] for an integrated luminosity of 1 fb^{-1} . We find satisfactory agreement. Following Ref. [13], we normalize our estimates for $Z + \text{jets}$ events and for $W + \text{jets}$ events to those of the ATLAS collaboration. The normalization factors are also shown in Table 1. Note that the normalization factor for the $Z(\nu\nu) + \text{jets}$ background (1.17) is consistent with Ref. [13], where it is estimated to be 1.2.

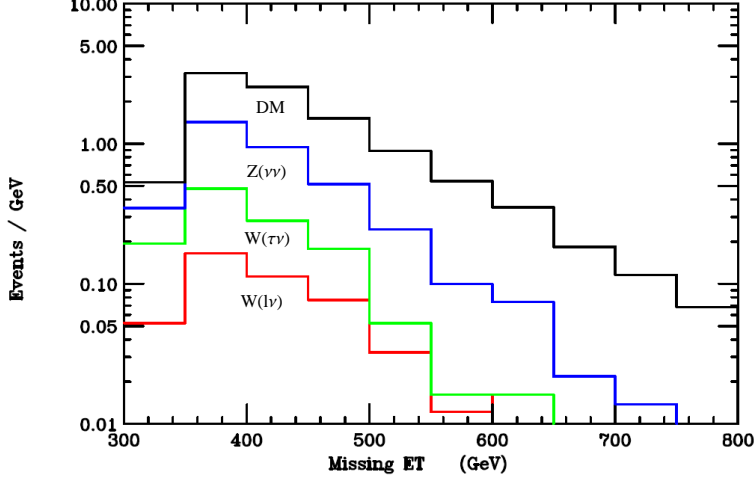


Figure 1: The \cancel{E}_T distribution of the backgrounds and the DM signal for 1 fb^{-1} at ATLAS. The curves from bottom to top successively include the $W(e/\mu\nu) + \text{jets}$ background, the $W(\tau\nu) + \text{jets}$ background, the $Z(\nu\nu) + \text{jets}$ background, and the DM signal with $\Lambda = 400 \text{ GeV}$ and $m_\chi = 10 \text{ GeV}$. *i.e.*, the curve labelled “DM” corresponds to the sum of all the backgrounds and the DM signal.

The DM signal in mono-jet events arises mainly from the following subprocesses:

$$g u \rightarrow u \chi \bar{\chi}, \quad (6)$$

$$g d \rightarrow d \chi \bar{\chi}. \quad (7)$$

We simulate the DM contribution to mono-jet events by following the method we have adopted for the background simulations. We generate $pp \rightarrow \chi\bar{\chi} + 1, 2 \text{ jets}$ events at the matrix element level with the precuts $\cancel{E}_T > 200 \text{ GeV}$ and $k_T > 140 \text{ GeV}$ for the jets. Parton showering is simulated with a 200 GeV matching scale, and detector effects are simulated. We have also confirmed for the DM signal that the final results are not significantly affected by varying the matching scale around 200 GeV. Finally, we rescale our signal by a factor of 1.17; see Table 1.

In order to compare our results with those of Ref. [13], we estimate the DM signal with $\Lambda = 400 \text{ GeV}$, $g_U = g_D = g_Q = 1$ and $m_\chi = 10 \text{ GeV}$. We show the \cancel{E}_T distribution in Fig. 1. All the curves are in good agreement with those in Fig. 2 of Ref. [13]. The difference in the 300-350 GeV bin is likely due to the different modeling of parton showers.

To compare the lower bound on Λ from our analysis with that from Ref. [13], we derive the observed bound for $m_\chi = 10 \text{ GeV}$ and $g_U = g_D = g_Q = 1$. It should be noted that only when all three couplings of the effective Lagrangian in Eq. (1) are equal, do we have purely vector-like couplings for both up and down quarks, as assumed in Ref. [13]. Isospin violation with purely vector-like couplings is not compatible with electroweak symmetry. To place 90%

C.L. lower limits on Λ we require [13]

$$\chi^2 \equiv \frac{(N_{obs} - N_{DM}(\Lambda) - N_{SM})^2}{N_{DM}(\Lambda) + N_{SM} + \sigma_{SM}^2} < 2.71 , \quad (8)$$

where N_{obs} , N_{DM} and N_{SM} are the number of observed events, the expected number of signal events, and the SM expectation, respectively, and σ_{SM} is the uncertainty in N_{SM} . We adopt $N_{obs} = 167$ and $N_{SM} \pm \sigma_{SM} = 193 \pm 25$ as obtained by the ATLAS collaboration in 1 fb^{-1} of data. After rescaling, we find the number of signal events for $\Lambda = 400 \text{ GeV}$ to be $N_{DM} = 319$, which implies: $N_{DM}(\Lambda) = 319 \times (400 \text{ GeV} / \Lambda)^4$. Finally, using the criterion of Eq. (8), we obtain the 90% C.L. bound,

$$\Lambda > 783 \text{ GeV} . \quad (9)$$

On the other hand, Fig. 4 of Ref. [13] shows separate bounds on Λ for DM-up quark and DM-down quark interactions, which are both purely vector-like. These bounds can be translated into a bound on Λ for $g_U = g_D = g_Q = 1$:

$$\Lambda > (700^4 + 575^4)^{1/4} \text{ GeV} = 769 \text{ GeV} , \quad (10)$$

which is consistent with our estimate in Eq. (9). It is clear that our estimate of the number of signal events is consistent with that of Ref. [13].

For $g_U = 1$ and $g_D = g_Q = 0$, we derive the following bound on Λ using the data and the SM background estimates of the ATLAS collaboration [14]:

$$\Lambda > 599 \text{ GeV} . \quad (11)$$

3.2 Study for $\sqrt{s} = 14 \text{ TeV}$

In this subsection, we study the DM contribution and the SM background to the mono-jet cross section at the LHC with $\sqrt{s} = 14 \text{ TeV}$. We introduce the following cut, which we refer to as *MonoJ14TeV*:

- Require $\cancel{E}_T > 800 \text{ GeV}$.
- Highest p_T jet should satisfy $|\eta_1| < 2.0$ and $p_{T1} > 700 \text{ GeV}$.
- Event is vetoed if the second hardest jet satisfies $|\eta_2| < 4.5$, and $p_{T2} > 120 \text{ GeV}$ or $\Delta\phi(\vec{p}_{T2}, \vec{E}_T) < 0.5$.
- Event is vetoed if there is another jet that satisfies $|\eta| < 4.5$ and $p_T > 60 \text{ GeV}$.

- Event is vetoed if there is an electron that satisfies $|\eta_e| < 2.47$ and $p_{Te} > 20$ GeV.
- Event is vetoed if there is a muon that satisfies $|\eta_\mu| < 2.4$ and $p_{T\mu} > 10$ GeV.

In comparison to the ATLAS *veryHighPT* selection cut, we keep the lepton veto conditions and scale all the jet p_T cuts by a factor of 2, while the \cancel{E}_T cut is chosen to reduce the $Z(\nu\nu)$ + jet background more efficiently in order to increase the signal significance for smaller DM signal cross sections.

We estimate the $Z(\nu\nu)$ + jet background in a manner similar to that for $\sqrt{s} = 7$ TeV, by changing the precuts to $\cancel{E}_T > 600$ GeV and $k_T > 240$ GeV for the jets, and the matching scale to 340 GeV. After testing the stability of our estimate under variation of the precuts and the matching scale, we find that the Z + jets background cross section is

$$\sigma_{Z+jets}(MonoJ14TeV) = 12.8 \text{ fb} . \quad (12)$$

Similarly, we estimate the cross sections for the $W(\tau\nu)$ + jet and $W(l\nu)$ + jet backgrounds with the precuts $p_T^l > 600$ GeV and $k_T > 240$ GeV for the jets, and a matching scale of 340 GeV. We find

$$\sigma_{W(\tau\nu)+jets}(MonoJ14TeV) = 2.4 \text{ fb} , \quad (13)$$

$$\sigma_{W(l\nu)+jets}(MonoJ14TeV) = 2.4 \text{ fb} . \quad (14)$$

To estimate the DM signal contribution, we set $(g_Q, g_U, g_D) = (0, \cos\phi, \sin\phi)$ so that the magnitudes of the couplings are given by $1/\Lambda^2$, and the isospin violation is parametrized by the phase $-\pi/2 < \phi \leq \pi/2$. The up and down quark couplings have the same sign for $0 < \phi < \pi/2$, and opposite signs for $-\pi/2 < \phi < 0$. We repeat the simulation steps of the $\sqrt{s} = 7$ TeV case, by changing the precuts to $\cancel{E}_T > 600$ GeV and $k_T > 240$ GeV for the jets, and the matching scale to 340 GeV. We calculate the cross sections for various values of the DM mass m_χ and $\phi = \tan^{-1}(g_D/g_U)$. The results for three representative couplings, $\phi = 0$ ($g_U = 1$), $\phi = \pm\pi/4$ ($|g_U| = |g_D| = 1/\sqrt{2}$) and $\phi = \pi/2$ ($g_D = 1$) are listed in Table 2 in units of $(800 \text{ GeV}/\Lambda)^4 \text{ fb}$. The mono-jet cross section does not distinguish between the signs of the g_U and g_D couplings, and hence $\pm\phi$ give the same prediction.

4 Mono-photon + \cancel{E}_T

The mono-jet cross section alone does not contain information on ϕ . Therefore additional signals are needed, and we study the mono-photon plus \cancel{E}_T signal in this section. Since the

m_χ	$\phi = 0$	$\phi = \pm\pi/4$	$\phi = \pm\pi/2$
10 GeV	15.9	11.0	6.37
300 GeV	15.1	10.5	5.91
500 GeV	13.0	8.89	4.98

Table 2: DM signal cross sections (in units of $(800 \text{ GeV}/\Lambda)^4 \text{ fb}$) for $\sqrt{s} = 14 \text{ TeV}$ with the *MonoJ14TeV* cut, for various values of the DM mass m_χ and the ratio of the DM couplings parametrized by $\phi = \tan^{-1}(g_D/g_U)$.

photon coupling to the up quark is twice that to the down quark, we expect a strong dependence of the DM signal on $|\phi|$. We first focus on the $\sqrt{s} = 7 \text{ TeV}$ case and reproduce the results of Ref. [13]. We then proceed to the $\sqrt{s} = 14 \text{ TeV}$ case, and look for an appropriate selection cut at high energies and at high integrated luminosity.

4.1 Study for $\sqrt{s} = 7 \text{ TeV}$

Following Refs. [13, 16], we implement the following selection cut, which we call *MonoG7TeV*:

- Require a photon with $|\eta_\gamma| < 1.44$ and $p_{T\gamma} > 95 \text{ GeV}$.
- Require $\cancel{E}_T > 80 \text{ GeV}$.
- Event is vetoed if there is a jet with $|\eta_j| < 3.0$ and $p_{Tj} > 20 \text{ GeV}$.
- Event is vetoed if there is an isolated lepton with $p_{Tl} > 10 \text{ GeV}$ and $\Delta R(l, \gamma) \equiv \sqrt{(\eta_l - \eta_\gamma)^2 + (\phi_l - \phi_\gamma)^2} > 0.04$.

The leading background arises from $Z(\nu\nu) + \gamma$ events. In addition, $Z(\nu\nu) + \text{jet}$ events with the jet misidentified as a photon, and $W(e\nu)$ events with the electron misidentified as a photon also contribute to the background.

We simulate the $Z(\nu\nu) + \gamma$ background as follows. We first generate $Z(\nu\nu) + \gamma$ and $Z(\nu\nu) + \gamma + 1 \text{ jet}$ events at the matrix element level with the precuts $p_{T\gamma} > 60 \text{ GeV}$ for the photon and $k_T > 60 \text{ GeV}$ for the jet, and simulate parton showering by using k_T -jet matching with a matching scale of 84 GeV . After simulating the detector effects with PGS and imposing the selection cut, we obtain

$$\sigma_{Z\gamma}(\text{MonoG7TeV}) = 48.0 \text{ fb} . \quad (15)$$

This gives 54.7 events in 1.14 fb^{-1} of data, while the CMS collaboration estimates 36.4 events [16]. We therefore multiply the DM signal (which has a similar event topology as the $Z(\nu\nu) + \gamma$

background) by the ratio $36.4/54.7 = 0.67$. This rescaling reflects the additional criteria for photon identification specific to the CMS detector. Note that the factor of 0.67 is in agreement with the analysis in Ref. [13], which finds 0.71.

The DM signal arises mainly from the following subprocesses:

$$u \bar{u} \rightarrow \gamma \chi \bar{\chi}, \quad (16)$$

$$d \bar{d} \rightarrow \gamma \chi \bar{\chi}. \quad (17)$$

Setting $m_\chi = 10$ GeV and $g_U = g_D = g_Q = 1$, we generate $\chi\bar{\chi} + \gamma$ and $\chi\bar{\chi} + \gamma + 1$ jet events at the matrix element level with the same precuts as for the background, which are then processed to the parton showering simulation with the same matching scale and finally the detector simulation is done using PGS. In this way, we find the DM signal cross section before the rescaling to be

$$\sigma_{DM\gamma}(MonoG7TeV) = 63.3 \times (400 \text{ GeV}/\Lambda)^4 \text{ fb}. \quad (18)$$

To compare our analysis with that of Ref. [13], we estimate the 90% C.L. lower bound on Λ by using the criterion of Eq. (8). For N_{SM} and σ_{SM} , we adopt the numbers estimated by the CMS collaboration, which are $N_{SM} = 67.3$ and $\sigma_{SM} = 8.4$ in 1.14 fb^{-1} [16]. The CMS collaboration reports $N_{obs} = 80$ [16]. N_{DM} is estimated by multiplying Eq. (18) by the normalization factor, 0.67. We obtain the 90% C.L. bound,

$$\Lambda > 422 \text{ GeV}. \quad (19)$$

On the other hand, Fig. 8 of Ref. [13] shows separate bounds on DM-up quark and DM-down quark interactions. These bounds can be translated into a bound on Λ for the case, $g_U = g_D = g_Q = 1$:

$$\Lambda > (400^4 + 240^4)^{1/4} \text{ GeV} = 412 \text{ GeV}. \quad (20)$$

This is consistent with our result in Eq. (19).

4.2 Study for $\sqrt{s} = 14$ TeV

We introduce the following selection cut for the LHC with $\sqrt{s} = 14$ TeV, which we name *MonoG14TeV-a*:

- Require a photon with $|\eta_\gamma| < 1.44$ and $p_{T\gamma} > 140$ GeV.
- Require $\cancel{E}_T > 140$ GeV.

Cut	$\sigma_{Z\gamma}$	$\sigma_{DM\gamma}$	$\sigma_{DM\gamma}/\sqrt{\sigma_{Z\gamma} + \sigma_{DM\gamma}}$
<i>MonoG14TeV-a</i>	35.8	5.49	0.85
<i>MonoG14TeV-b</i>	11.6	3.34	0.87
<i>MonoG14TeV-c</i>	4.51	2.13	0.83

Table 3: Cross sections (in fb) and significance factors ($\text{fb}^{1/2}$) for the DM signal with $m_\chi = 10$ GeV, $\Lambda = 800$ GeV and $\phi = \pi/4$. The three selection cuts for mono-photon events are compared.

- Event is vetoed if there is a jet with $|\eta_j| < 3.0$ and $p_{Tj} > 40$ GeV.
- Event is vetoed if there is an isolated lepton with $p_{Tl} > 10$ GeV and $\Delta R(l, \gamma) > 0.04$.

We also introduce the selection cut *MonoG14TeV-b* which requires $(p_{T\gamma}, \cancel{E}_T) > (200, 200)$ GeV, and the cut *MonoG14TeV-c* which requires $(p_{T\gamma}, \cancel{E}_T) > (260, 260)$ GeV, and for which all the other requirements are the same as for *MonoG14TeV-a*.

We estimate the $Z(\nu\nu) + \gamma$ background in a similar manner to the case of $\sqrt{s} = 7$ TeV, by changing the precuts to $p_{T\gamma} > 100$ GeV for the photon and $k_T > 100$ GeV for the jet, and the matching scale to 140 GeV. We estimate the DM signal contribution with the same precuts and matching scale as for the $Z(\nu\nu) + \gamma$ background estimation for $\sqrt{s} = 14$ TeV.

Table 3 shows the cross sections and significance factors ($S/\sqrt{S+B}$) for the DM signal with $m_\chi = 10$ GeV, $\Lambda = 800$ GeV and $\phi = \pi/4$, where the three selection cuts are imposed. The numbers are in units of fb for the cross sections and $\text{fb}^{1/2}$ for the significance factor. We find that the significance factor does not depend much on the choice of the selection cut. This is because the background cross section decreases by a factor of 8 and the signal also decreases by $2.6 \simeq \sqrt{8}$ when we change the cut from *MonoG14TeV-a* to *MonoG14TeV-c*. For our study, we adopt the selection cut *MonoG14TeV-a* which yields the largest signal cross section. This is because, with more events, it is easier to discriminate the signal from the background from the difference in their \cancel{E}_T and $p_{T\gamma}$ distributions as well as from the correlation between γ and \cancel{E}_T momenta, although we do not perform such an analysis in this paper.

In Fig. 2, we show the cross sections for the $Z + \gamma$ background and the DM signal for $\Lambda = 800$ GeV and $(g_Q, g_U, g_D) = (0, \cos\phi, \sin\phi)$ that satisfy the cut *MonoG14TeV-a*. The three curves correspond to $m_\chi = 10, 300, 500$ GeV. The mono-photon cross section does not depend on the signs of the g_U and g_D couplings, and hence $\pm\phi$ give the same prediction.

In Table 4, we present the DM signal cross sections in units of $(800 \text{ GeV}/\Lambda)^4 \text{ fb}$ for $\phi = 0, \pm\pi/4$ and $\pi/2$. Roughly speaking, the $\phi = \pi/2$ ($g_D = 1$) case gives about a factor of 7 smaller DM signal cross section than the $\phi = 0$ ($g_U = 1$) case, while the cross section in the $\phi = \pm\pi/4$ ($|g_U| = |g_D| = 1/\sqrt{2}$) case is about half of that in the $\phi = 0$ case, for all m_χ

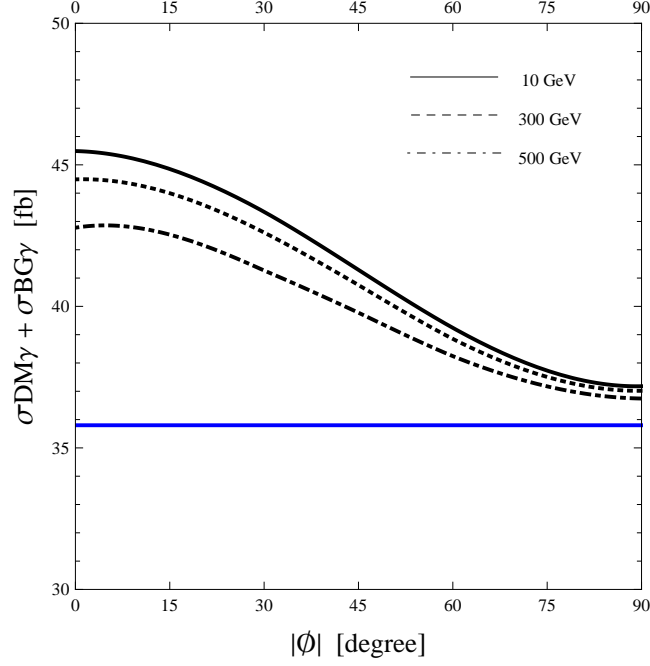


Figure 2: The $Z + \gamma$ background cross section and the DM signal cross section for $\Lambda = 800$ GeV that satisfy the *MonoG14TeV-a* criteria, as a function of $|\phi|$ for the couplings $(g_Q, g_U, g_D) = (0, \cos \phi, \sin \phi)$. The horizontal solid line corresponds to the background cross section. The curves correspond to the background + signal cross sections for three values of m_χ .

m_χ	$\phi = 0$	$\phi = \pm\pi/4$	$\phi = \pm\pi/2$
10 GeV	9.69	5.49	1.38
300 GeV	8.69	4.96	1.22
500 GeV	6.98	3.98	0.945

Table 4: DM signal cross sections (in units of $(800 \text{ GeV}/\Lambda)^4 \text{ fb}$) for $\sqrt{s} = 14$ TeV that satisfy the *MonoG14TeV-a* cut.

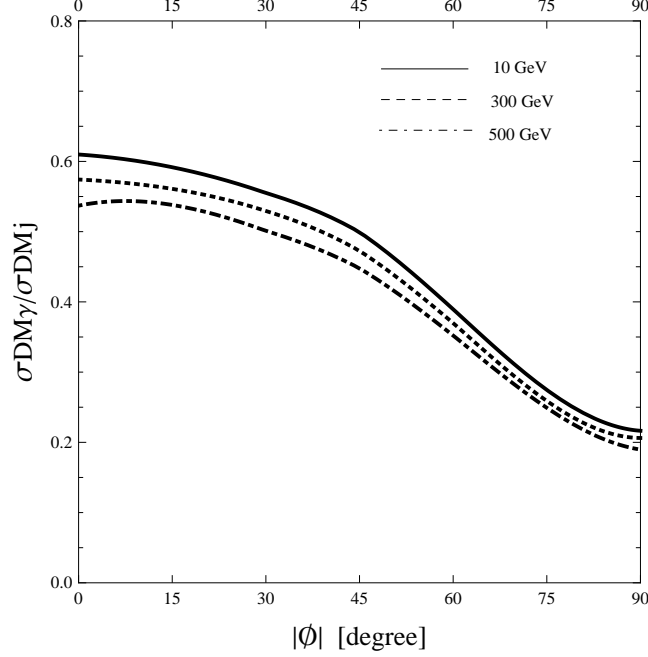


Figure 3: Ratio of the DM signal cross section in the mono-photon channel with the *MonoG14TeV-a* cut to the cross section in the mono-jet channel with the *MonoJ14TeV* cut for three values of m_χ .

between 10 GeV and 500 GeV. This reflects the combined effect of the QED coupling ratio $(Q_d/Q_u)^2 = 1/4$ and the ratio of the down quark to up quark parton distribution functions in pp collisions.

In Fig. 3, we show the ratio of the DM signal cross sections in the mono-photon channel with the *MonoG14TeV-a* cut to the cross section in the mono-jet channel with the *MonoJ14TeV* cut. We find that this ratio is very sensitive to the coupling ratio $|g_D/g_U| = \tan|\phi|$, but insensitive to the DM mass m_χ . It is independent of Λ and $\sqrt{g_U^2 + g_D^2}$.

Experimentally, the cross section ratio, $\sigma_{DM\gamma}/\sigma_{DMj}$, is determined by

$$\frac{\sigma_{DM\gamma}(\text{monophoton cut})}{\sigma_{DMj}(\text{monojet cut})} = \frac{(N_{obs}^\gamma - N_{SM}^\gamma)(\text{monophoton cut})}{(N_{obs}^j - N_{SM}^j)(\text{monojet cut})}, \quad (21)$$

where N_{obs}^γ and N_{obs}^j are the observed number of mono-photon and mono-jet events, respectively, and N_{SM}^γ and N_{SM}^j are the SM expectations for mono-photon background events and mono-jet background events, respectively. Since the cross section ratio has a common value for a wide range of m_χ , we can determine the value of $|\phi|$ by comparing the observed value of the cross section ratio with Fig. 3.

As an illustration, we estimate the integrated luminosity L needed to measure the cross section ratio with 10% accuracy close to the point $|\phi| = \pi/4$ for $\Lambda = 800$ GeV and $m_\chi = 10$ GeV. We assume that the statistical uncertainty of the number of events, N , follows $\Delta N = \sqrt{N}$, and ignore systematic uncertainties. To estimate N_{obs}^γ and N_{SM}^γ , we rescale the cross sections by the normalization factor 0.67 obtained in Section 4.1. The statistical uncertainty of $\sigma_{DM\gamma}/\sigma_{DMj}$ is given by

$$\Delta \left(\frac{\sigma_{DM\gamma}}{\sigma_{DMj}} \right) = \left(\frac{\sigma_{DM\gamma}}{\sigma_{DMj}} \right) \sqrt{ \frac{N_{obs}^j + N_{SM}^j}{(N_{obs}^j - N_{SM}^j)^2} + \frac{N_{obs}^\gamma + N_{SM}^\gamma}{(N_{obs}^\gamma - N_{SM}^\gamma)^2} }. \quad (22)$$

Inserting $N_{SM}^\gamma = L \times 0.67 \times 35.8$ fb and $N_{obs}^\gamma - N_{SM}^\gamma = L \times 0.67 \times 5.49$ fb from Table 3, $N_{SM}^j = L \times (12.8 + 2.4 + 2.4)$ fb from Eqs. (12-14), and $N_{obs}^j - N_{SM}^j = L \times 11.0$ fb from Table 2, we find that in order to obtain a 10% measurement of the monophoton-to-monojet cross section ratio, $L \simeq 420$ fb $^{-1}$ is needed.

We now evaluate the integrated luminosity needed to establish the isospin violating nature of the DM-quark couplings as a function of Λ . As an example, consider the ability to reject the hypothesis that isospin is conserved *i.e.*, $\phi = \pi/4$ ($g_U = g_D = 1/\sqrt{2}$), given that $\phi = 0$ ($g_U = 1, g_D = 0$). The DM mass m_χ is fixed at 10 GeV. To reject the hypothesis at 3σ , from Fig. 3 we require

$$\begin{aligned} \Delta \left(\frac{\sigma_{DM\gamma}}{\sigma_{DMj}} \right) (\phi = 0) &= \frac{1}{3} \left(\frac{\sigma_{DM\gamma}}{\sigma_{DMj}} (\phi = 0) - \frac{\sigma_{DM\gamma}}{\sigma_{DMj}} (\phi = \pi/4) \right) \\ &= 0.037. \end{aligned} \quad (23)$$

Then using Eqs. (22) and (23), in Fig. 4 we show the integrated luminosity needed to reject the isospin-conservation hypothesis at the 3σ C.L., $L_{3\sigma}$, as a function of the contact interaction scale Λ .

5 Di-jet + \cancel{E}_T

Since the mono-jet and mono-photon cross sections depend only on the absolute values of g_U and g_D , a measurement of the relative sign of g_U and g_D is not possible from these channels. To determine the relative sign, we now focus on events with two hard jets and large \cancel{E}_T . This channel can be sensitive to the relative sign of the g_U and g_D couplings because in the subprocess,

$$u_R d_R \rightarrow u_R d_R \chi \bar{\chi}, \quad (24)$$

the amplitudes where $\chi \bar{\chi}$ are emitted from the up quark interfere with the amplitudes where $\chi \bar{\chi}$ are emitted from the down quark, as can be seen from the Feynman diagrams in Fig. 5.

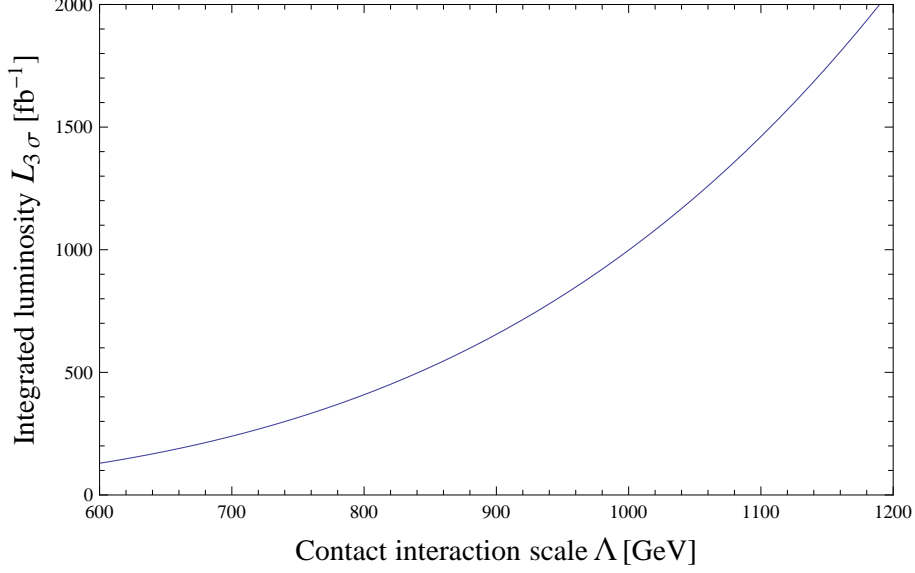


Figure 4: Integrated luminosity $L_{3\sigma}$ needed to reject the isospin-conservation hypothesis, $\phi = \pi/4$ ($g_U = g_D = 1/\sqrt{2}$), at 3σ given that $\phi = 0$ ($g_U = 1$, $g_D = 0$). Here, $m_\chi = 10$ GeV. Only statistical uncertainties are taken into account.

The interference term is directly proportional to $g_U g_D$ so that the cross section depends on the sign of $g_U g_D$.

5.1 Extracting the Interference

In this subsection we discuss kinematic conditions that enhance interference effects in the diagrams of Fig. 5.

5.1.1 Suppressing contributions from quark-gluon collisions

First, it is necessary to suppress large contributions from quark-gluon collisions,

$$q g \rightarrow q g Z(\nu\nu), \quad (25)$$

$$q g \rightarrow q g \chi\bar{\chi}, \quad (q = u, d). \quad (26)$$

While the subprocesses in Eq. (25) give the dominant background for the DM plus di-jet production events, the subprocesses in Eq. (26) should also be suppressed because their cross sections do not depend on $g_U g_D$. The contributions from quark-gluon collisions can be reduced, compared to the signal subprocess in Eq. (24) from quark-quark collisions by imposing a very large cut on the “di-jet cluster transverse mass” [17]:

$$M_T(jj; \cancel{E}_T) \equiv \sqrt{M_{12}^2 + |\vec{p}_{1T} + \vec{p}_{2T}|^2} + \cancel{E}_T, \quad (27)$$

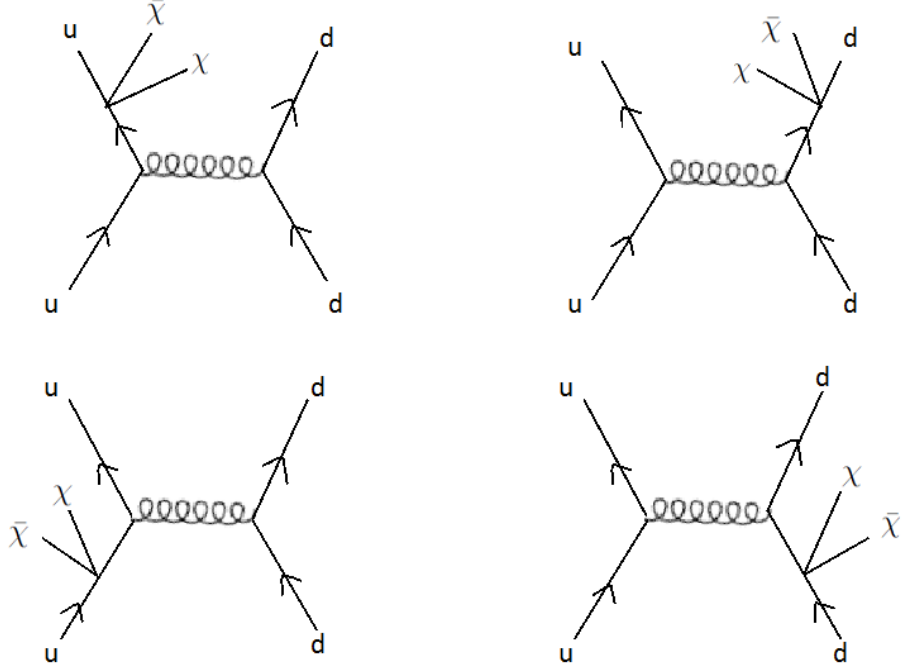


Figure 5: Feynman diagrams for the subprocess, $u_R d_R \rightarrow u_R d_R \chi \bar{\chi}$. The diagrams on the left are proportional to g_U , and the ones on the right are proportional to g_D .

where M_{12} is the invariant mass of the two hardest jets, and $\vec{p}_{1T} + \vec{p}_{2T}$ is the vector sum of the transverse momenta of the two hardest jets. Since the parton center-of-mass energy ($\sqrt{\hat{s}}$) is always larger than $M_T(jj; \cancel{E}_T)$, by imposing a cut on $M_T(jj; \cancel{E}_T)$, we can select those events that satisfy

$$\sqrt{\hat{s}} \geq M_T(jj; \cancel{E}_T) > (M_T(jj; \cancel{E}_T))^{cut}. \quad (28)$$

By choosing a large value for $(M_T(jj; \cancel{E}_T))^{cut}$, we can suppress the contributions from quark-gluon collisions relative to those from quark-quark collisions, because the former subprocesses have relatively less parton center-of-mass energy. We note that the contributions from the same quark collisions:

$$q \bar{q} \rightarrow q \bar{q} Z(\nu\nu), \quad (29)$$

$$q \bar{q} \rightarrow q \bar{q} \chi \bar{\chi}, \quad (q = u, d), \quad (30)$$

cannot be suppressed by a cut on $M_T(jj; \cancel{E}_T)$. We therefore treat them as irreducible backgrounds for a measurement of the sign of $g_U g_D$.

5.1.2 Utilizing the generalized null radiation zone theorem

Generally speaking, when a subprocess contains two Feynman diagrams that interfere, the ratio of the interference term to the cross section is maximized when the amplitudes of the two diagrams take the same absolute value. The null radiation zone theorem [18] provides us with powerful criteria for identifying such kinematic regions. The theorem states that for any tree-level Feynman diagram, if the ratio $Q_k/(p_k \cdot q)$ (where Q_k is the charge of an external particle, p_k is its four-momentum, and q is the four-momentum of the emitted photon) is the same for all external particles and if the charge Q_k 's are conserved, then the sum of the amplitudes of all the tree-level diagrams made by adding one photon emission vertex to the original diagram vanishes for all helicities. Since the amplitude for each diagram does not vanish, the theorem implies that the amplitudes of the contributing diagrams cancel exactly, *i.e.*, they interfere maximally. The original theorem applies to massless vector boson emission via a vector coupling to fermions. We make use of the theorem for our dark matter pair which couples to quarks via vector and axial vector couplings. Since the dark matter pair is not massless, we first generalize the theorem to emission of a massive vector current.

We now show that the null radiation zone theorem can be generalized to emission of a massive vector boson, or a vector current whose invariant mass squared is time-like, $q^2 > 0$. Consider the following process in which a neutral vector current, V , is emitted:

$$a + b \rightarrow 1 + 2 + \dots + n + V. \quad (31)$$

We label the particle four-momenta and charges in the initial state by p_i , Q_i ($i = a, b$), and those in the final state by p_f , Q_f ($f = 1, 2, \dots, n$). We denote the four-momentum of the vector current by q . The tree-level scattering amplitude should vanish for all helicities when the following conditions are satisfied:

$$\frac{Q_i}{2p_i \cdot q - q^2} = \frac{Q_f}{2p_f \cdot q + q^2} = (\text{a common value}) \quad \text{for all } i \text{ and } f, \quad (32)$$

$$\sum_i Q_i = \sum_f Q_f. \quad (33)$$

Let us focus on the four diagrams of Fig. 5. We denote the four-momenta of the incoming quarks by k_1 and k_2 , those of the outgoing quarks by p_1 and p_2 and the four-momentum sum of the DM momenta by q . We notice that the values of $2p_1 \cdot q + q^2$ and $2p_2 \cdot q + q^2$ are always positive. The values of $2k_1 \cdot q - q^2$ and $2k_2 \cdot q - q^2$ can take both signs, but their sum is always positive because $k_1 + k_2 = p_1 + p_2 + q$. Therefore the null radiation zone can be realized only when g_U and g_D take the same sign. We thus expect that the interference in pp collisions is destructive if g_U and g_D take the same sign, and is constructive otherwise.

The theorem suggests that if the condition,

$$k_1 \cdot q - \frac{q^2}{2} = k_2 \cdot q - \frac{q^2}{2} = p_1 \cdot q + \frac{q^2}{2} = p_2 \cdot q + \frac{q^2}{2}, \quad (34)$$

is satisfied, the amplitudes of the four diagrams of Fig. 5 cancel completely for $g_U = g_D$, while the sum of the amplitudes is maximally enhanced for $g_U = -g_D$. Equation (34) reduces to the following kinematic conditions for massless partons satisfying $p_1^2 = p_2^2 = k_1^2 = k_2^2 = 0$:

$$|\vec{p}_1| = |\vec{p}_2|, \quad (35)$$

$$q^2 = 0, \quad (36)$$

where $|\vec{p}_1|$ and $|\vec{p}_2|$ are respectively the magnitudes of the three-momenta of p_1 and p_2 in the *colliding parton center-of-mass* frame. Since our DM particle is not massless, the condition Eq. (34) cannot be satisfied and the null radiation zone does not exist in the physical region. However, we expect that strong destructive interference occurs for $g_U = g_D$ when the condition Eq. (34) is approximately satisfied.

At hadron colliders, we cannot measure the missing mass $\sqrt{q^2}$, and cannot determine the colliding parton center-of-mass frame. Therefore, to enhance kinematic regions around the null radiation zone, we must make use of the constraints among jet transverse momenta coming from Eq. (35). In the following we examine the selection cut,

$$|p_{T1} - p_{T2}| < C p_{T1}, \quad (37)$$

where p_{T1} and p_{T2} are the transverse momenta of the hardest and second hardest jets, respectively, and C is a number less than unity. Although no selection cut can be applied to enhance kinematic regions that nearly satisfy Eq. (34), such regions are automatically favored in pp collisions with a fixed cut because they are the regions where the parton center-of-mass energy is minimized.

5.2 Analysis

The “signal” in this analysis is not DM production itself, but the difference in the DM signal cross sections for $g_U/g_D > 0$ and $g_U/g_D < 0$. In this analysis, therefore, we consider the value of $\sigma_{DMjj}(\phi = -\pi/4) - \sigma_{DMjj}(\phi = \pi/4)$ as the signal and treat the value of $\sigma_{DMjj}(\phi = -\pi/4) + \sigma_{SM}$ as the background.

We first examine selection cuts dubbed *DiJ-a*, *DiJ-b*, *DiJ-c* and *DiJ-d*. The *DiJ-a* cut is:

- Require two jets with $|\eta| < 4.5$ and $p_T > 200$ GeV.
- Require $\cancel{E}_T > 300$ GeV.

- Require $M_T(jj; \cancel{E}_T) = \sqrt{M_{12}^2 + |\vec{p}_{1T} + \vec{p}_{2T}|^2} + \cancel{E}_T > 2 \text{ TeV}$.
- Event is vetoed if there is another jet that satisfies $|\eta| < 4.5$ and $p_T > 100 \text{ GeV}$.
- Event is vetoed if there is a jet whose three-momentum \vec{p} satisfies $\Delta\phi(\vec{p}, \vec{\cancel{E}}_T) < 0.2$.

The first, second and fourth conditions define the two jets plus large \cancel{E}_T events that we study. It is the third condition that enhances events from quark-quark collisions over those from quark-gluon collisions. The last condition is necessary to reduce those $Z(\nu\nu) + \text{jets}$ events in which a quark emits the Z boson almost collinearly; the amplitude receives collinear enhancement even for the Z boson because $E_{jet}/M_Z \gg 1$. For comparison, we consider a selection cut *DiJ-b* that requires $M_T(jj; \cancel{E}_T) > 2.5 \text{ TeV}$, and a selection cut *DiJ-c* that requires $M_T(jj; \cancel{E}_T) > 3 \text{ TeV}$, with the other conditions the same as for *DiJ-a*. Based on the null radiation zone theorem, we also consider a selection cut *DiJ-d* that requires

$$|p_{T1} - p_{T2}| < 0.5 p_{T1}, \quad (38)$$

in addition to the conditions of *DiJ-b*. (p_{T1} and p_{T2} are the transverse momenta of the hardest and second hardest jets, respectively.) The cuts are summarized as follows:

$$DiJ - a : M_T(jj; \cancel{E}_T) > 2 \text{ TeV} . \quad (39)$$

$$DiJ - b : M_T(jj; \cancel{E}_T) > 2.5 \text{ TeV} . \quad (40)$$

$$DiJ - c : M_T(jj; \cancel{E}_T) > 3 \text{ TeV} . \quad (41)$$

$$DiJ - d : M_T(jj; \cancel{E}_T) > 2.5 \text{ TeV} \quad \text{and} \quad |p_{T1} - p_{T2}| < 0.5 p_{T1} . \quad (42)$$

Our simulation of the SM background only accounts for the dominant background from $Z(\nu\nu) + \text{jets}$ events. To estimate the background cross section, we generate $Z(\nu\nu) + 2, 3$ jets events at the matrix element level with the following precuts: $\cancel{E}_T > 200 \text{ GeV}$, $k_T > 160 \text{ GeV}$, $\Delta R(\vec{p}_j, \vec{p}_Z) > 0.2$, $\sqrt{\hat{s}} > 2 (2.5) \text{ TeV}$ when using the *DiJ-a* cut (*DiJ-b*, *DiJ-c* and *DiJ-d* cuts), where \vec{p}_j is the three-momentum of any jet and \vec{p}_Z that of the Z boson. We match the matrix element events with the parton shower with a matching scale of 220 GeV , and perform a detector simulation. We find that the cross section after the final cut does not change drastically when the matching scale is varied by $\pm 40 \text{ GeV}$.

The DM production cross section is estimated in a similar manner; we generate $\chi\bar{\chi} + 2, 3$ jets events with the same precuts as the background simulation (\vec{p}_Z is replaced with the three-momentum sum of the DM momenta), and process them to parton showering and detector simulation with the same matching scale.

Table 5 shows the cross sections and the significance factors ($S/\sqrt{S+B}$) for DM production with $m_\chi = 10 \text{ GeV}$, $\Lambda = 800 \text{ GeV}$ and $\phi = \pm\pi/4$, for the four selection cuts. Also shown is the

Cut	σ_{Zjj}	$\sigma_{DMjj}(\phi = \frac{\pi}{4})$	$\sigma_{DMjj}(\phi = -\frac{\pi}{4})$	$\frac{\sigma_{DMjj}(-\pi/4) - \sigma_{DMjj}(\pi/4)}{\sigma_{DMjj}(-\pi/4)}$	$\frac{\sigma_{DMjj}(-\pi/4) - \sigma_{DMjj}(\pi/4)}{\sqrt{\sigma_{Zjj} + \sigma_{DMjj}(-\pi/4)}}$
<i>DiJ-a</i>	49.8	9.246	9.595	0.0364	0.0453
<i>DiJ-b</i>	20.1	4.094	4.355	0.0599	0.0528
<i>DiJ-c</i>	8.34	1.868	1.999	0.0655	0.0407
<i>DiJ-d</i>	13.7	1.847	2.012	0.0820	0.0416

Table 5: Cross sections (in fb), the dimensionless ratio of the interference effect to the DM production cross section, and the significance factor ($\text{fb}^{1/2}$) for DM production with $m_\chi = 10$ GeV, $\Lambda = 800$ GeV and $\phi = \pm\pi/4$, for four different cuts.

m_χ	$\phi = +\pi/4$	$\phi = -\pi/4$
10 GeV	4.094	4.355
300 GeV	3.712	3.895

Table 6: DM production cross sections (in units of $(800 \text{ GeV}/\Lambda)^4 \text{ fb}$) for $\sqrt{s} = 14$ TeV that satisfy the *DiJ-b* selection cut.

ratio of the interference effect ($\sigma_{DMjj}(\phi = -\pi/4) - \sigma_{DMjj}(\phi = +\pi/4)$) to the DM production cross section for $\phi = -\pi/4$ ($\sigma_{DMjj}(\phi = -\pi/4)$). Notice that in this analysis the “signal” cross section corresponds to the difference between the DM cross sections for $\phi = \pi/4$ and $\phi = -\pi/4$. The numbers are in units of fb for the cross sections and $\text{fb}^{1/2}$ for the significance factors. From Table 5 we see that the *DiJ-b* cut gives the largest significance factor. We note in passing that the requirement Eq. (38) of the *DiJ-d* cut, which is based on the null radiation zone theorem, does enhance the ratio of the interference effect to the DM production cross section, $\{\sigma_{DMjj}(\phi = -\pi/4) - \sigma_{DMjj}(\phi = +\pi/4)\}/\sigma_{DMjj}(\phi = -\pi/4)$. Unfortunately, the $Z + \text{jets}$ background is not significantly diminished by this requirement, resulting in a significance factor that is smaller for the *DiJ-d* cut than for the *DiJ-b* cut.

In Fig. 6 and Table 6, we show cross sections for the $Z + \text{jets}$ background and the DM production process for $\Lambda = 800$ GeV and $m_\chi = 10, 300$ GeV that satisfy the *DiJ-b* selection cut. The numbers in the table are in units of $(800 \text{ GeV}/\Lambda)^4 \text{ fb}$. Finally in Fig. 7, we show the ratio of the DM signal cross section in the di-jet channel with the *DiJ-b* cut to the cross section in the mono-jet channel with the *MonoJ14TeV* cut, as a function of ϕ .

5.3 Discussion of the Di-jet Channel

From Fig. 6 and Table 6, we confirm that the Feynman diagrams of the subprocess, $u_R d_R \rightarrow \chi \bar{\chi} u_R d_R$, interfere destructively if g_U and g_D have the same sign, and constructively if they have opposite signs. This is in accordance with our expectation in Section 5.1 based on the

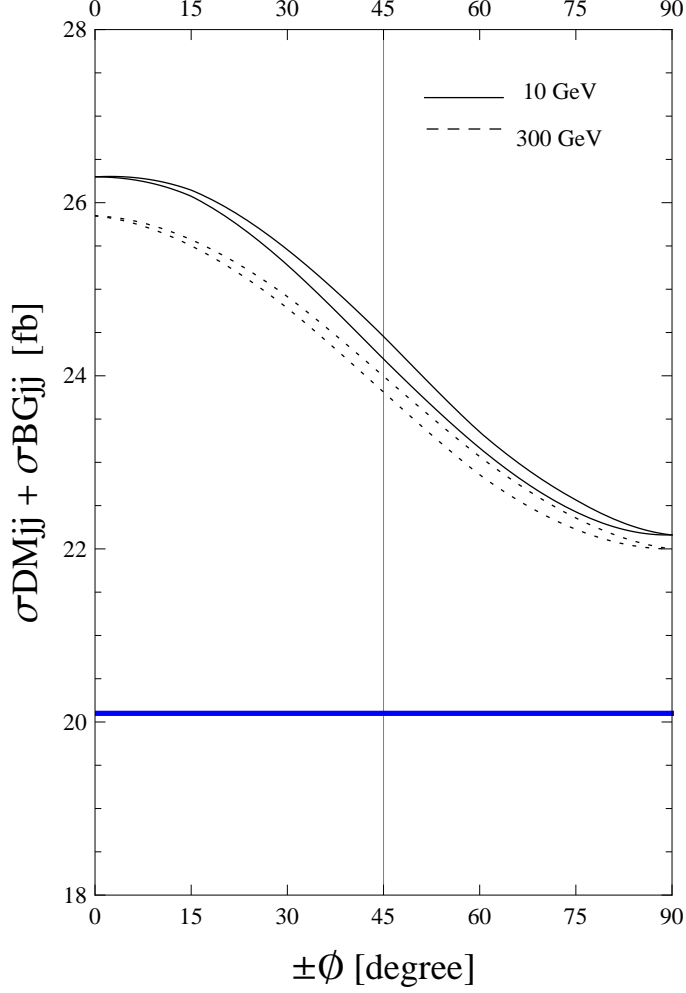


Figure 6: The $Z + \text{jets}$ background cross section and the DM production cross section for $\Lambda = 800$ GeV that satisfy the $DiJ\text{-}b$ selection cut, as a function of ϕ for the couplings $(g_Q, g_U, g_D) = (0, \cos \phi, \sin \phi)$. The horizontal solid line corresponds to the background cross section. The solid and dotted curves correspond to the background + signal cross sections for $m_\chi = 10$ GeV and 300 GeV, respectively. For each pair of curves, the upper one corresponds to $\phi < 0$ and the lower one to $\phi > 0$.

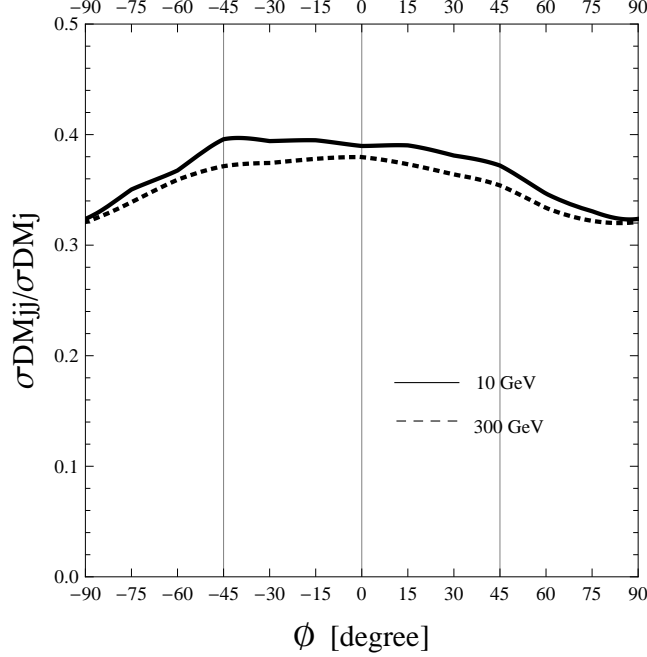


Figure 7: Ratio of the DM production cross section in the di-jet channel with the *DiJ-b* cut to the cross section in the mono-jet channel with the *MonoJ14TeV* cut for two values of m_χ .

null radiation zone theorem [18]. Table 6 also indicates that the effect of the interference is diminished for larger DM masses. This is because for heavier DM, the physical region deviates more from the null radiation zone given by Eq. (34).

The deviation of Fig. 7 from a left-right symmetric form is a consequence of the interference. Apart from the left-right asymmetry, Fig. 7 shows that the cross section ratio is smaller for $\phi \simeq \pm\pi/2$ than for $\phi \simeq 0$. This is due to the difference in the parton distribution functions of the up and down quarks; since the momentum distribution of the down quark in a proton leans towards a smaller momentum region compared to that of the up quark, events involving only down quarks have relatively less parton center-of-mass energy and are more likely to be rejected by the high cut on $M_T(jj; \cancel{E}_T)$.

Once it has been experimentally established that $|g_U| \simeq |g_D|$ ($|\phi| \simeq \pi/4$), and that $m_\chi \sim 10$ GeV, the sign of $g_U g_D$ can be determined by measuring the following DM cross section ratio and comparing it with the prediction of Fig. 7:

$$\frac{\sigma_{DMjj}}{\sigma_{DMj}} = \frac{(N_{obs}^{jj} - N_{SM}^{jj})(DiJ-b)}{(N_{obs}^j - N_{SM}^j)(MonoJ14TeV)}, \quad (43)$$

where N_{obs}^{jj} is the observed number of di-jet events and N_{SM}^{jj} is the SM expectation for di-jet events.

We estimate the integrated luminosity needed to determine the sign of $g_U g_D$ for $\Lambda = 800$ GeV, $m_\chi = 10$ GeV and $|\phi| = \pi/4$. To distinguish $\phi = -\pi/4$ from $\phi = +\pi/4$ at the 2σ level, the dijet-to-monojet cross section ratio must be measured with 3% accuracy since Table 5 shows that the difference between the 2 cases is about 6%. The statistical uncertainty of $\sigma_{DMjj}/\sigma_{DMj}$ is given by

$$\Delta \left(\frac{\sigma_{DMjj}}{\sigma_{DMj}} \right) = \left(\frac{\sigma_{DMjj}}{\sigma_{DMj}} \right) \sqrt{ \frac{N_{obs}^j + N_{SM}^j}{(N_{obs}^j - N_{SM}^j)^2} + \frac{N_{obs}^{jj} + N_{SM}^{jj}}{(N_{obs}^{jj} - N_{SM}^{jj})^2} } . \quad (44)$$

Inserting $N_{SM}^{jj} = L \times 20.1$ fb and $N_{obs}^{jj} - N_{SM}^{jj} = L \times 4.355$ fb from Table 5, and $N_{SM}^j = L \times (12.8 + 2.4 + 2.4)$ fb from Eqs. (12-14) and $N_{obs}^j - N_{SM}^j = L \times 11.0$ fb from Table 2, we find that to achieve a 3% measurement of the dijet-to-monojet cross section ratio, $L \simeq 3000 \text{ fb}^{-1}$ is needed.

6 Dark matter with suppressed scattering on xenon

We now derive constraints on the contact interaction scale Λ of our model Eq. (1) for couplings that evade bounds from the xenon-based LUX direct detection experiment [6]. At present, LUX imposes a strong constraint on the spin-independent cross section for DM-nucleus elastic scattering. Since the DM candidate of our model is a Dirac fermion, LUX imposes a severe lower bound on the contact interaction scale Λ (for g_Q, g_U, g_D normalized as $g_Q^2 + g_U^2 + g_D^2 = 1$) for general values of the ratios of g_Q, g_U and g_D . For example, for $g_Q = g_U = 0$ and $g_D = 1$, the lower bound on Λ from the LUX data far exceeds 10 TeV for $10 \text{ GeV} \lesssim m_\chi \lesssim 500 \text{ GeV}$. However, for $g_Q = 0$ and $g_D/g_U = -0.89$, the bound becomes significantly weaker because contributions from the DM-up quark coupling and DM-down quark coupling mostly cancel for the proton and neutron content of Xe isotopes. In this section, we take $g_Q = 0$ and $g_D/g_U = -0.89$, so that constraints from the LUX and XENON 100 [4] experiments are weakened. With this choice of couplings, we obtain LHC bounds on the contact interaction scale by normalizing the coupling constants as $g_U^2 + g_D^2 = 1$. We employ the latest results of the CMS collaboration from mono-jet searches with 19.5 fb^{-1} of data at the 8 TeV LHC [19], and mono-photon searches redone with 5.0 fb^{-1} of data at the 7 TeV LHC [20]. Bounds on Λ derived from the di-jet channel are weaker than those from the mono-jet channel.

To derive bounds from the CMS mono-jet data, we calculate the DM signal cross section in the following way. We generate $pp \rightarrow \chi\bar{\chi} + 1, 2 \text{ jets}$ events with the pp center-of mass energy of 8 TeV at the matrix element level with the precuts $\cancel{E}_T > 200$ GeV and $k_T > 140$ GeV for

the jets. Parton showering is simulated with a 200 GeV matching scale, and detector effects are simulated. We implement the following selection cut, *LATEST-MONOT*, that mimics the one used in Ref. [19]:

- Require $\cancel{E}_T > 400$ GeV.
- Highest p_T jet should satisfy $|\eta_1| < 2.4$ and $p_{T1} > 110$ GeV.
- If a second highest p_T jet with $|\eta_2| < 4.5$ exists, the azimuthal angle between this jet and the highest p_T jet should satisfy $\Delta\phi(j_1, j_2) < 2.5$.
- Event is vetoed if three or more jets satisfy $|\eta| < 4.5$ and $p_T > 30$ GeV.
- Event is vetoed if there is an electron that satisfies $|\eta_e| < 2.47$ and $p_{Te} > 10$ GeV.
- Event is vetoed if there is a muon that satisfies $|\eta_\mu| < 2.4$ and $p_{T\mu} > 10$ GeV.

To calibrate the DM signal cross section calculated above, we calculate the cross section for the $Z(\nu\nu) + \text{jets}$ background (that has similar kinematics to the DM signal process), in the same way as the DM signal cross section. We compare this cross section with the $Z(\nu\nu) + \text{jets}$ background cross section evaluated by CMS collaboration [19] which is (2596/19.5) fb, and then rescale the DM signal cross section by their ratio.

Using Eq. (8), we obtain the 90% C.L. lower bound on Λ with 19.5 fb^{-1} of data for each value of the DM mass m_χ . Here $N_{DM}(\Lambda)$, which scales as $1/\Lambda^4$, is the number of DM signal events that is based on the DM signal cross section derived and calibrated above. The number of observed events N_{obs} , the number of expected SM events N_{SM} and its uncertainty, σ_{SM} , are reported by the CMS collaboration to be 3677, 3663, and 196, respectively [19].

A bound from CMS mono-photon data is derived in a similar fashion. To calculate the DM signal cross section we generate $pp \rightarrow \chi\bar{\chi} + \gamma$, $\chi\bar{\chi} + \gamma + 1 \text{ jet}$ events with the pp center-of-mass energy of 7 TeV at the matrix element level with the precuts $p_{T\gamma} > 60$ GeV for the photon and $k_T > 60$ GeV for the jet, and simulate parton showering with a matching scale of 84 GeV. Finally, detector simulations are performed. We implement the following selection cut, *LATEST-MONOG*, that mimics the one used in Ref. [20]:

- Require a photon with $|\eta_\gamma| < 1.44$ and $p_{T\gamma} > 145$ GeV.
- Require $\cancel{E}_T > 130$ GeV.
- Event is vetoed if there is a jet with $|\eta_j| < 3.0$, $p_{Tj} > 40$ GeV and $\Delta R(j, \gamma) < 0.5$.

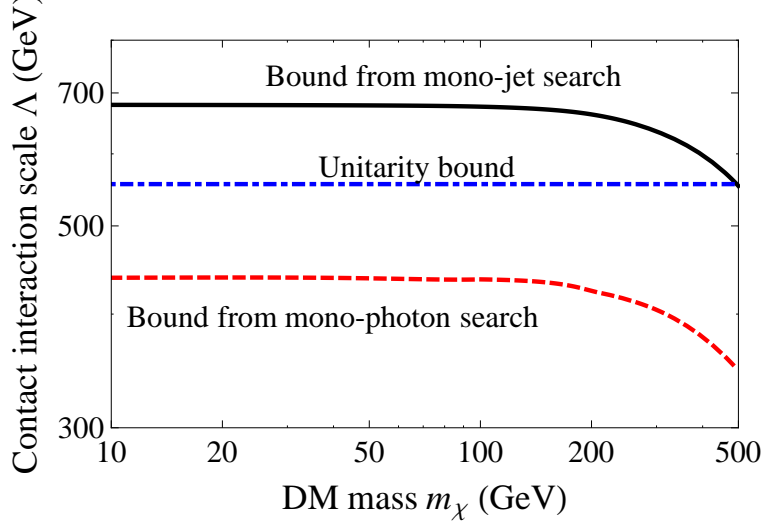


Figure 8: 90% C.L. lower bounds on the contact interaction scale Λ for $g_Q = 0$, $g_U = 0.75$, $g_D = -0.66$, derived from the latest CMS mono-jet [19] and mono-photon [20] data. Note that with this choice of couplings, the DM scattering cross section in xenon-based detectors like LUX is significantly suppressed. Also shown is the lower bound required by perturbative unitarity of the process $u_R \bar{u}_R \rightarrow \chi \bar{\chi}$ with a parton center-of-mass energy of $\sqrt{\hat{s}} = 3$ TeV.

- Event is vetoed if there is an isolated lepton with $p_{Tl} > 20$ GeV and $\Delta R(l, \gamma) > 0.04$.

The DM signal cross section derived above is calibrated in the same way as for the mono-jet search. We calculate the cross section for the $Z(\nu\nu) + \gamma$ background in the same way as the DM signal, compare this cross section with the $Z(\nu\nu) + \gamma$ background cross section evaluated by the CMS collaboration [20] which is (45.3/5.0) fb, and then rescale the DM signal cross section by their ratio.

We derive the 90% C.L. lower bound on Λ with 5.0 fb^{-1} of data using Eq. (8). Here $N_{DM}(\Lambda)$ is the number of DM signal events that is based on the DM signal cross section derived and calibrated above, and N_{obs} , N_{SM} and σ_{SM} are 75, 75.1 and 9.4, respectively [20].

In Fig. 8, we display 90% C.L. lower bounds on the contact interaction scale Λ for $g_Q = 0$, $g_U = 0.75$, $g_D = -0.66$ (which corresponds to $g_D/g_U = -0.89$, $g_U^2 + g_D^2 = 1$) for various m_χ . For comparison, we also show the lower bound on Λ required by absolute perturbative unitarity of the process $u_R \bar{u}_R \rightarrow \chi \bar{\chi}$ for $g_U = 0.75$ with a parton center-of-mass energy, $\sqrt{\hat{s}} = 3$ TeV. (The unitarity bound for the process $d_R \bar{d}_R \rightarrow \chi \bar{\chi}$ for $g_D = -0.66$ is weaker.) Details of absolute perturbative unitarity are explained in the Appendix.

7 Mediator effects

We now consider how the presence of a mediator field that contributes to resonant DM production changes our results. We introduce a vector field, V_μ , with TeV scale mass that couples to SM quarks and DM through the following Lagrangian:

$$\mathcal{L}_{mediator} = (\bar{g}_U \bar{u}_R \gamma_\mu u_R + \bar{g}_D \bar{d}_R \gamma_\mu d_R + \bar{g}_\chi \bar{\chi} \gamma_\mu \chi) V^\mu - \frac{1}{2} M_V^2 V^\mu V_\mu. \quad (45)$$

For large M_V , we recover the interaction term of Eq. (1) (with $g_Q = 0$) with the correspondence:

$$\frac{\bar{g}_U \bar{g}_\chi}{M_V^2} = \frac{g_U}{\Lambda^2}, \quad \frac{\bar{g}_D \bar{g}_\chi}{M_V^2} = \frac{g_D}{\Lambda^2}. \quad (46)$$

If V_μ has a mass of several TeV, the DM production cross section at the LHC is enhanced by the V_μ resonance. We calculate how the cross sections for mono-jet, mono-photon and di-jet events depend on M_V .

For our numerical study, we require the coupling constants \bar{g}_U , \bar{g}_D and \bar{g}_χ to satisfy

$$\frac{\bar{g}_U \bar{g}_\chi}{M_V^2} = \frac{\bar{g}_D \bar{g}_\chi}{M_V^2} = \frac{1}{\sqrt{2}} \frac{1}{(800 \text{ GeV})^2}, \quad (47)$$

so that in the absence of the V_μ resonance, we obtain a contact interaction with $\Lambda = 800 \text{ GeV}$ and $g_U = g_D = 1/\sqrt{2}$. This allows us to quantify the effect of the mediator. We select the following V_μ masses:

$$M_V = 2.0 \text{ TeV}, \quad 2.4 \text{ TeV}, \quad 3.2 \text{ TeV}. \quad (48)$$

We do not consider values of $M_V \lesssim 1.6 \text{ TeV}$ because these are excluded by the 8 TeV LHC data [21] for coupling constants satisfying Eq. (47). We choose values of $\bar{g}_U (= \bar{g}_D)$ and \bar{g}_χ so that the decay width of V_μ is minimized and the resonant production of χ is maximally enhanced. Since the width of V_μ is given by

$$\Gamma_V = \frac{3\bar{g}_U^2 + 3\bar{g}_D^2 + 2\bar{g}_\chi^2}{24\pi} M_V, \quad (49)$$

the width is minimized if $\bar{g}_\chi = \sqrt{3}\bar{g}_U$ for $\bar{g}_U = \bar{g}_D$.

We evaluate the cross sections for mono-jet events at the LHC with $\sqrt{s} = 8 \text{ TeV}$ and 14 TeV, mono-photon events at 14 TeV and di-jet events at 14 TeV. For mono-jet events at 8 TeV, we implement a cut that resembles the $SR4$ selection cut used by the ATLAS collaboration [21], and compare the cross sections in our benchmark models with the ATLAS data [21]. Our cut, $MonoJ8TeV$, is as follows:

	$M_V = 2.0$ TeV	$M_V = 2.4$ TeV	$M_V = 3.2$ TeV	Contact interaction
$\sigma(MonoJ8TeV)$	6.33	3.72	-	-
$\sigma(MonoJ14TeV)$	27.1	17.5	7.48	11.0
$\sigma(MonoG14TeV-a)$	12.4	8.15	3.53	5.49
$\sigma(DiJ-b)$	10	6.0	2.6	4.09

Table 7: Cross sections (in fb) for mono-jet events at the 8 TeV LHC, and mono-jet, mono-photon and di-jet events at the 14 TeV LHC (for the cuts specified), for models with a mediator of mass M_V and minimum width, and for a contact interaction.

- Require one jet with $|\eta| < 2.0$ and $p_T > 500$ GeV.
- Require $\cancel{E}_T > 500$ GeV.
- Event is vetoed if three or more jets satisfy $|\eta| < 4.5$ and $p_T > 30$ GeV.
- Event is vetoed if there is an electron that satisfies $|\eta_e| < 2.47$ and $p_{Te} > 20$ GeV.
- Event is vetoed if there is a muon that satisfies $|\eta_\mu| < 2.4$ and $p_{T\mu} > 7$ GeV.

We simulate the signal $pp \rightarrow \chi\bar{\chi} + jets$ events using the procedure described in Section 3, with the precuts $k_T > 180$ GeV and $\cancel{E}_T > 300$ GeV, and a 250 GeV matching scale, which we have confirmed to be appropriate. We analogously simulate $pp \rightarrow Z(\nu\nu) + jets$ events and compare the cross section after the *MonoJ8TeV* cut with the one after the *SR4* cut estimated by the ATLAS collaboration [21]. We find that the two cross sections match, so we do not need to rescale our signal cross section. Using the number of observed events (N_{obs}) and the background prediction ($N_{SM} \pm \sigma_{SM}$) reported in Ref. [21], and our estimate of N_{DM} for a particular M_V , we employ the criterion of Eq. (8) to assess if the value of M_V is allowed at 90% C.L. We find $\chi^2(M_V = 2 \text{ TeV}) = 2.15$ and $\chi^2(M_V = 2.4 \text{ TeV}) = 1.54$. No signal events are produced for $M_V = 3.2$ TeV at the 8 TeV LHC. Thus $M_V > 2$ TeV is unconstrained by current LHC data.

We implement the *MonoJ14TeV*, *MonoG14TeV-a* and *DiJ-b* cuts for mono-jet, mono-photon and di-jet events at the 14 TeV LHC, respectively. The cross sections are displayed in Table 7. We see that the cross sections at the 14 TeV LHC are significantly enhanced for a ~ 2 TeV mass mediator. The cross sections for a 3.2 TeV mediator are reduced because the width of the mediator satisfying Eq. (47) is as large as its mass.

8 Discussion and Conclusion

We explored ways of observing the isospin violating nature of a dark matter particle at the LHC. We pursued the possibility that DM interacts with SM quarks via couplings that violate

isospin by considering a toy model. We adopted a Dirac fermion DM particle that couples to up and down quarks through contact interactions with different strengths. The cross section ratio of the DM production associated with a hard jet and that with a photon reflects the absolute value of the ratio of the DM couplings to up and down quarks because they have different electric charges. We showed that this ratio can be measured at the LHC by observing and comparing mono-photon + \cancel{E}_T events with mono-jet + \cancel{E}_T events.

The relative sign of the DM couplings to up and down quarks can be studied only by comparing the cross section of DM production associated with two hard jets to that with one hard jet. This is because the subprocess, $u_R d_R \rightarrow u_R d_R \chi \bar{\chi}$, that contributes to di-jet + \cancel{E}_T events, contains an interference term that is proportional to $g_U g_D$. In order to extract the interference term, we implemented a very hard cut on the di-jet cluster transverse mass, $M_T(jj; \cancel{E}_T)$, which selects quark-quark collision events over quark-gluon collision backgrounds. We showed that the effect of the interference does in fact appear in the cross section of di-jet + \cancel{E}_T events with the sign expected from the null radiation zone theorem [18], and that it is possible to determine the relative sign of the couplings by observing and comparing di-jet + \cancel{E}_T events with mono-jet + \cancel{E}_T events.

In Sections 3, 4, 5 and 6, we studied the scenario in which the DM couples to quarks through contact interactions of dimension-6. In the Appendix we show that in this scenario, the perturbative unitarity bound for the DM production process is violated when the DM invariant mass is large. We therefore assumed that the DM production cross section is constant when the DM invariant mass is larger than the absolute perturbative unitarity bound of Eq. (2). However, the DM production cross section in pp collisions at the 14 TeV LHC is only slightly affected by this modification because the number of events in which the DM invariant mass is larger than the unitarity bound is exponentially suppressed by the parton distribution functions of the proton.

In Section 7, we considered a model with a mediator field, and studied how the cross sections change with the mass of the mediator. We showed that the cross sections for mono-jet, mono-photon and di-jet events at the 14 TeV LHC can be enhanced by the mediator resonance without conflicting with mono-jet searches at the 8 TeV LHC [21]. Prospects for discovery improve if the DM and quarks couple through a ~ 2 TeV mediator, instead of via contact interactions.

Throughout, we focused on the case with $g_Q = 0$. If $g_Q \neq 0$, the DM cross section ratios in

Figs. 3 and 7, will be modified. For Fig. 3, the angle ϕ will be replaced by

$$\phi_{eff} = \tan^{-1} \left(\sqrt{g_D^2 + g_Q^2} / \sqrt{g_U^2 + g_Q^2} \right) .$$

On the other hand, Fig. 7 will be modified in a complicated way. Note that the ratio of the di-jet and mono-jet signal cross sections can be written in the following way when $g_Q = 0$:

$$\sigma_{jj}/\sigma_j = \frac{Cg_U^2 + Dg_Ug_D + Eg_D^2}{Ag_U^2 + Bg_D^2} , \quad (50)$$

where A, B, C, D, E are numerical factors with $A, B, C, E > 0$ and $D < 0$ as we saw in Section 5. For $g_Q \neq 0$, the expression above becomes:

$$\sigma_{jj}/\sigma_j = \frac{C(g_U^2 + g_Q^2) + D(g_Ug_D + g_Qg_U + g_Qg_D) + E(g_D^2 + g_Q^2)}{A(g_U^2 + g_Q^2) + B(g_D^2 + g_Q^2)} . \quad (51)$$

Our analysis can be generalized to the entire parameter space of (g_Q, g_U, g_D) .

Although this work is motivated by isospin violating dark matter, our methods are applicable to other new physics models for which one studies the ratio of the new physics couplings to up and down quarks. The di-jet channel is challenging because it is necessary to suppress large contributions from gluon-quark interactions. However, it is the only channel that is sensitive to the relative sign of the up and down quark couplings, and hence should be studied seriously once new physics that couples to quarks is discovered. We believe that our exploratory studies will be useful to probe new physics properties at the LHC.

Acknowledgments

D.M. thanks the KEK Theory Center, where this work was initiated, for its support and hospitality. He also thanks the Center for Theoretical Underground Physics and Related Areas (CETUP* 2012) in South Dakota for its support and hospitality during the completion of this work. T.Y. thanks the organizers and the lecturers of “KIAS School on MadGraph for LHC Physics Simulation” (24-29 October, 2011) [22], where physics simulation tools used in this study were introduced. This work was supported in part by Grant-in-Aids for Scientific Research (Nos. 23-3599, 20340064 and 23104006) from the Japan Society for the Promotion of Science, and by US DOE grants DE-FG02-04ER41308 and DE-FG02-13ER42024, and US NSF grant PHY-0544278.

Appendix: Unitarity bounds for contact interactions

Unitarity of scattering amplitudes

We begin with a review of unitarity constraints on general scattering amplitudes. The S-matrix can be written as

$$S \equiv 1 + iT, \quad (52)$$

where T gives the transition amplitudes. In terms of T , the unitarity of the S-matrix, $S^\dagger S = 1$, is

$$-i(T - T^\dagger) = T^\dagger T. \quad (53)$$

For an elastic scattering process $A + B \rightarrow A + B$, the above equation gives

$$\begin{aligned} & -i(\langle \vec{p}_A \vec{p}_B | T | \vec{k}_A \vec{k}_B \rangle - \langle \vec{p}_A \vec{p}_B | T^\dagger | \vec{k}_A \vec{k}_B \rangle) \\ &= \langle \vec{p}_A \vec{p}_B | T^\dagger T | \vec{k}_A \vec{k}_B \rangle \\ &= \sum_{\{q_i\}} \left(\prod_i \int \frac{d^3 \vec{q}_i}{(2\pi)^3 2q_i^0} \right) \langle \vec{p}_A \vec{p}_B | T^\dagger | \{\vec{q}_i\} \rangle \langle \{\vec{q}_i\} | T | \vec{k}_A \vec{k}_B \rangle, \end{aligned} \quad (54)$$

where $|\{\vec{q}_i\}\rangle$ constitute a complete set of states. The scattering matrix element, \mathcal{M} , for the scattering process,

$$A + B \rightarrow 1 + 2 + \dots + F, \quad (55)$$

can be expressed as

$$i\mathcal{M}(\vec{k}_A \vec{k}_B \rightarrow \vec{p}_1 \vec{p}_2 \dots \vec{p}_F) (2\pi)^4 \delta^4(k_A + k_B - p_1 - p_2 \dots - p_F) \equiv \langle \vec{p}_1 \vec{p}_2 \dots \vec{p}_F | iT | \vec{k}_A \vec{k}_B \rangle, \quad (56)$$

where we denote the three- and four-momenta of the initial-state particles by \vec{k}_A , \vec{k}_B and k_A , k_B , respectively, and those of the final-state particles by \vec{p}_1 , \vec{p}_2 , ..., \vec{p}_F and p_1 , p_2 , ..., p_F . In terms of matrix elements, the unitarity relation Eq. (54) reads

$$\begin{aligned} & -i \left\{ \mathcal{M}(\vec{k}_A \vec{k}_B \rightarrow \vec{p}_A \vec{p}_B) - \mathcal{M}(\vec{p}_A \vec{p}_B \rightarrow \vec{k}_A \vec{k}_B)^* \right\} \\ &= \sum_{\{q_i\}} \left(\prod_i \int \frac{d^3 \vec{q}_i}{(2\pi)^3 2q_i^0} \right) \mathcal{M}(\vec{p}_A \vec{p}_B \rightarrow \{\vec{q}_i\})^* \mathcal{M}(\vec{k}_A \vec{k}_B \rightarrow \{\vec{q}_i\}) (2\pi)^4 \delta^4 \left(k_A + k_B - \sum_i q_i \right). \end{aligned} \quad (57)$$

The unitarity bounds for both elastic and inelastic scattering processes follow from Eq. (57).

Absolute perturbative unitarity bound for DM production

We are interested in the perturbative unitarity bound for the DM production process arising from the contact interaction terms in Eq. (1),

$$q_R^{c1} \bar{q}_{Rc1} \rightarrow \chi \bar{\chi} \quad (q = u, d), \quad (58)$$

where $c1$ is a color index. In this subsection, we discuss the *absolute* unitarity bound for the above process which holds regardless of the details of other processes, such as $q\bar{q} \rightarrow q'\bar{q}'$ and $\chi\bar{\chi} \rightarrow \chi\bar{\chi}$. For simplicity, we assume that the quarks and the DM are massless. If the DM has a non-negligible mass, the unitarity bound weakens.

Consider the elastic scattering processes, $q_R^{c1} \bar{q}_{Rc1} \rightarrow q_R^{c2} \bar{q}_{Rc2}$ ($q = u, d$), whose matrix elements we denote by \mathcal{M}_{qq} . Also consider inelastic scattering processes, $q_R^{c1} \bar{q}_{Rc1} \rightarrow \chi_R \bar{\chi}_R$ and $q_R^{c1} \bar{q}_{Rc1} \rightarrow \chi_L \bar{\chi}_L$, whose matrix elements we denote by $\mathcal{M}_{q\chi_R}$ and $\mathcal{M}_{q\chi_L}$, respectively. From Eq. (57), we find

$$\begin{aligned} & -i \left\{ \mathcal{M}_{qq}(\vec{k}_A \vec{k}_B \rightarrow \vec{p}_A \vec{p}_B) - \mathcal{M}_{qq}(\vec{p}_A \vec{p}_B \rightarrow \vec{k}_A \vec{k}_B)^* \right\} \\ \geq & \int \frac{d^3 \vec{q}_1}{(2\pi)^3 2q_1^0} \int \frac{d^3 \vec{q}_2}{(2\pi)^3 2q_2^0} \mathcal{M}_{qq}(\vec{p}_A \vec{p}_B \rightarrow \vec{q}_1 \vec{q}_2)^* \mathcal{M}_{qq}(\vec{k}_A \vec{k}_B \rightarrow \vec{q}_1 \vec{q}_2) (2\pi)^4 \delta^4(k_A + k_B - q_1 - q_2) \\ & + \int \frac{d^3 \vec{q}_1}{(2\pi)^3 2q_1^0} \int \frac{d^3 \vec{q}_2}{(2\pi)^3 2q_2^0} \mathcal{M}_{q\chi_R}(\vec{p}_A \vec{p}_B \rightarrow \vec{q}_1 \vec{q}_2)^* \mathcal{M}_{q\chi_R}(\vec{k}_A \vec{k}_B \rightarrow \vec{q}_1 \vec{q}_2) (2\pi)^4 \delta^4(k_A + k_B - q_1 - q_2) \\ & + (\mathcal{M}_{q\chi_R} \rightarrow \mathcal{M}_{q\chi_L}) \\ = & \frac{1}{(2\pi)^{24} q_1^0 q_2^0} \int d\Omega |\vec{q}| \frac{q_1^0 q_2^0}{q_1^0 + q_2^0} \mathcal{M}_{qq}(\vec{p}_A \vec{p}_B \rightarrow \vec{q}_1 \vec{q}_2)^* \mathcal{M}_{qq}(\vec{k}_A \vec{k}_B \rightarrow \vec{q}_1 \vec{q}_2) \\ & + \frac{1}{(2\pi)^{24} q_1^0 q_2^0} \int d\Omega |\vec{q}| \frac{q_1^0 q_2^0}{q_1^0 + q_2^0} \mathcal{M}_{q\chi_R}(\vec{p}_A \vec{p}_B \rightarrow \vec{q}_1 \vec{q}_2)^* \mathcal{M}_{q\chi_R}(\vec{k}_A \vec{k}_B \rightarrow \vec{q}_1 \vec{q}_2) \\ & + (\mathcal{M}_{q\chi_R} \rightarrow \mathcal{M}_{q\chi_L}), \end{aligned} \quad (59)$$

where Ω is the scattering solid angle in the center-of-mass frame, and $\mathcal{M}_{q\chi_R} \rightarrow \mathcal{M}_{q\chi_L}$ is the term obtained by replacing $\mathcal{M}_{q\chi_R}$ by $\mathcal{M}_{q\chi_L}$ in the previous term. We make a partial wave expansion of \mathcal{M}_{qq} as

$$\mathcal{M}_{qq}(s, \cos \alpha) \equiv 16\pi \sum_{l=0} a_l^{qq}(s) (2l+1) P_l(\cos \alpha), \quad (60)$$

where s is the center-of-mass energy and α is the scattering angle in the center-of-mass frame. Expanding the last two lines of Eq. (59) in terms of $P_l(\cos \theta)$, where θ is the angle between \vec{p}_A

and \vec{k}_A in the center-of-mass frame:

$$\begin{aligned}
& \frac{1}{(2\pi)^2 4q_1^0 q_2^0} \int d\Omega |\vec{q}| \frac{q_1^0 q_2^0}{q_1^0 + q_2^0} \mathcal{M}_{q\chi_R}(\vec{p}_A \vec{p}_B \rightarrow \vec{q}_1 \vec{q}_2)^* \mathcal{M}_{q\chi_R}(\vec{k}_A \vec{k}_B \rightarrow \vec{q}_1 \vec{q}_2) \\
& \equiv 16\pi \sum_{l=0} b_l^{q\chi_R}(s) (2l+1) P_l(\cos \theta), \\
& + (R \rightarrow L).
\end{aligned} \tag{61}$$

Then Eq. (59) becomes

$$2\text{Im}(a_l^{qq}) \geq 2|a_l^{qq}|^2 + b_l^{q\chi_R} + b_l^{q\chi_L}, \tag{62}$$

which leads to the following bound on the matrix elements for the processes $\chi_R \bar{\chi}_R \rightarrow q_R \bar{q}_R$ and $\chi_L \bar{\chi}_L \rightarrow q_R \bar{q}_R$:

$$b_l^{q\chi_R} + b_l^{q\chi_L} \leq \frac{1}{2}. \tag{63}$$

To obtain the unitarity bound we evaluate $b_l^{q\chi}$'s perturbatively. At the tree level, we have

$$\begin{aligned}
b_0^{q\chi_R} &= b_0^{q\chi_L} = \frac{1}{192\pi^2} \frac{s^2 g_q^2}{\Lambda^4}, \\
b_1^{q\chi_R} &= b_1^{q\chi_L} = \frac{1}{3 \cdot 192\pi^2} \frac{s^2 g_q^2}{\Lambda^4}, \\
b_{l \geq 2}^{q\chi_R} &= b_{l \geq 2}^{q\chi_L} = 0 \quad (q = u, d).
\end{aligned} \tag{64}$$

We thus find that Eq. (63) is satisfied if the center-of-mass energy, $\sqrt{s} = M_{q\bar{q}} = M_{\chi\bar{\chi}}$, obeys the condition,

$$\sqrt{s} < (48\pi^2)^{1/4} \frac{\Lambda}{\sqrt{g_q}} = 3.7 \text{ TeV} \times \left(\frac{\Lambda}{800 \text{ GeV}} \right) \left(\frac{1}{g_q} \right)^{1/2} \tag{65}$$

for $q = u, d$.

One can also derive a perturbative unitarity bound for DM production by considering the elastic scattering process, $\chi \bar{\chi} \rightarrow \chi \bar{\chi}$, instead of $q_R^{c1} \bar{q}_{Rc1} \rightarrow q_R^{c2} \bar{q}_{Rc2}$. However, the resultant bound is weaker than Eq. (65).

Model-dependent perturbative unitarity bound for DM production

In this subsection, we derive the perturbative unitarity bound for DM production *with specific assumptions* on the underlying model. Our assumptions are:

- DM and quarks interact through contact terms in the Lagrangian,

$$\begin{aligned}
\mathcal{L}_{contact} = & \frac{\bar{g}_\chi^2}{M_V^2} (\bar{\chi}\gamma^\mu\chi) (\bar{\chi}\gamma_\mu\chi) \\
& + \frac{\bar{g}_\chi\bar{g}_U}{M_V^2} (\bar{\chi}\gamma^\mu\chi) (\bar{u}_R\gamma_\mu u_R) + \frac{\bar{g}_\chi\bar{g}_D}{M_V^2} (\bar{\chi}\gamma^\mu\chi) (\bar{d}_R\gamma_\mu d_R) \\
& + \frac{\bar{g}_U^2}{M_V^2} (\bar{u}_R\gamma^\mu u_R) (\bar{u}_R\gamma_\mu u_R) + \frac{\bar{g}_U\bar{g}_D}{M_V^2} (\bar{u}_R\gamma^\mu u_R) (\bar{d}_R\gamma_\mu d_R) \\
& + \frac{\bar{g}_D^2}{M_V^2} (\bar{d}_R\gamma^\mu d_R) (\bar{d}_R\gamma_\mu d_R), \tag{66}
\end{aligned}$$

which naturally arises by integrating out a massive mediator vector field that couples to u_R , d_R and χ .

- Interactions between DM particles and between DM and a quark are induced only by terms in Eq. (66).
- Interactions between quarks are induced only by terms in Eq. (66), and by SM gauge interactions.

We note that the contact terms in Eq. (66) correspond to those in Eq. (1) according to Eq. (46).

We denote the matrix elements for scattering processes involving the DM and/or quarks, $A\bar{A} \rightarrow B\bar{B}$ ($A, B = u_R^{c1}, d_R^{c2}, \chi_R, \chi_L$), by \mathcal{M}^{AB} , and expand in partial waves,

$$\mathcal{M}^{AB}(s, \cos\alpha) = 16\pi \sum_{l=0} a_l^{AB}(s)(2l+1) P_l(\cos\alpha). \tag{67}$$

For each l , consider a matrix of the factors $a_l^{AB}(s)$, given by

$$\mathcal{T}_l \equiv \begin{pmatrix} a_l^{u_R u_R} & a_l^{u_R d_R} & a_l^{u_R \chi_R} & a_l^{u_R \chi_L} \\ a_l^{d_R u_R} & a_l^{d_R d_R} & a_l^{d_R \chi_R} & a_l^{d_R \chi_L} \\ a_l^{\chi_R u_R} & a_l^{\chi_R d_R} & a_l^{\chi_R \chi_R} & a_l^{\chi_R \chi_L} \\ a_l^{\chi_L u_R} & a_l^{\chi_L d_R} & a_l^{\chi_L \chi_R} & a_l^{\chi_L \chi_L} \end{pmatrix}, \tag{68}$$

where the color indices in a_l^{AB} 's are implicit. We diagonalize \mathcal{T}_l 's by taking linear combinations of the initial and final states to find the eigenvalues t_l^i ($i = 1, 2, \dots, 8$). For each l , the scattering

processes involving the DM and/or quarks can be regarded as the elastic scatterings of the states in the new basis. From Eq. (57), it follows that each t_l^i satisfies

$$\text{Im}(t_l^i) \geq |t_l^i|^2, \quad (69)$$

which leads to the bound,

$$|t_l^i| \leq 1. \quad (70)$$

The model-dependent unitarity bound is derived by evaluating t_l^i 's perturbatively, based on the assumptions above. At the tree level, we have

$$\begin{aligned} a_0^{u_R^c u_R^c} &= \frac{1}{16\pi} \frac{\bar{g}_U^2}{M_V^2} s + \frac{1}{16\pi} \frac{1}{3} g_s^2 \\ a_0^{u_R^c d_R^c} &= a_0^{d_R^c u_R^c} = \frac{1}{16\pi} \frac{\bar{g}_U \bar{g}_D}{M_V^2} s + \frac{1}{16\pi} \frac{1}{3} g_s^2 \\ a_0^{d_R^c d_R^c} &= \frac{1}{16\pi} \frac{\bar{g}_D^2}{M_V^2} s + \frac{1}{16\pi} \frac{1}{3} g_s^2 \\ a_0^{\chi_R u_R} &= a_0^{\chi_L u_R} = a_0^{u_R \chi_R} = a_0^{u_R \chi_L} = \frac{1}{16\pi} \frac{\bar{g}_U \bar{g}_\chi}{M_V^2} s \\ a_0^{\chi_R d_R} &= a_0^{\chi_L d_R} = a_0^{d_R \chi_R} = a_0^{d_R \chi_L} = \frac{1}{16\pi} \frac{\bar{g}_D \bar{g}_\chi}{M_V^2} s \\ a_0^{\chi_R \chi_R} &= a_0^{\chi_R \chi_L} = a_0^{\chi_L \chi_R} = a_0^{\chi_L \chi_L} = \frac{1}{16\pi} \frac{\bar{g}_\chi^2}{M_V^2} s \\ a_1^{u_R^c u_R^c} &= \frac{1}{16\pi} \frac{1}{3} \frac{\bar{g}_U^2}{M_V^2} s + \frac{1}{16\pi} \frac{1}{3 \cdot 3} g_s^2 \\ a_1^{u_R^c d_R^c} &= a_1^{d_R^c u_R^c} = \frac{1}{16\pi} \frac{1}{3} \frac{\bar{g}_U \bar{g}_D}{M_V^2} s + \frac{1}{16\pi} \frac{1}{3 \cdot 3} g_s^2 \\ a_1^{d_R^c d_R^c} &= \frac{1}{16\pi} \frac{1}{3} \frac{\bar{g}_D^2}{M_V^2} s + \frac{1}{16\pi} \frac{1}{3 \cdot 3} g_s^2 \\ -a_1^{\chi_R u_R} &= a_1^{\chi_L u_R} = -a_1^{u_R \chi_R} = a_1^{u_R \chi_L} = \frac{1}{16\pi} \frac{1}{3} \frac{\bar{g}_U \bar{g}_\chi}{M_V^2} s \\ -a_1^{\chi_R d_R} &= a_1^{\chi_L d_R} = -a_1^{d_R \chi_R} = a_1^{d_R \chi_L} = \frac{1}{16\pi} \frac{1}{3} \frac{\bar{g}_D \bar{g}_\chi}{M_V^2} s \\ -a_1^{\chi_R \chi_R} &= -a_1^{\chi_L \chi_L} = a_1^{\chi_R \chi_L} = a_1^{\chi_L \chi_R} = \frac{1}{16\pi} \frac{1}{3} \frac{\bar{g}_\chi^2}{M_V^2} s \\ a_{l \geq 2}^{AB} &= 0, \end{aligned} \quad (71)$$

where g_s is the $\text{SU}(3)_C$ gauge coupling. We neglected electroweak gauge interactions, which give subdominant contributions relative to the $\text{SU}(3)_C$ gauge interaction.

As an example, for $M_V = 800$ GeV, $\bar{g}_U = \bar{g}_D = 1/\sqrt{2}$ and $\bar{g}_\chi = 1$, for each l and i Eq. (70) is satisfied if

$$\sqrt{s} \lesssim 2.5 \text{ TeV} . \quad (72)$$

References

- [1] J. L. Feng, J. Kumar, D. Marfatia and D. Sanford, Phys. Lett. B **703**, 124 (2011) [arXiv:1102.4331 [hep-ph]].
- [2] R. Bernabei *et al.* [DAMA Collaboration], Eur. Phys. J. C **56**, 333 (2008) [arXiv:0804.2741 [astro-ph]].
- [3] C. E. Aalseth *et al.* [CoGeNT Collaboration], Phys. Rev. Lett. **106**, 131301 (2011) [arXiv:1002.4703 [astro-ph.CO]].
- [4] E. Aprile, *et al.* [XENON100 Collaboration], arXiv:1207.5988 [astro-ph.CO]; Phys. Rev. Lett. **107**, 131302 (2011) [arXiv:1104.2549 [astro-ph.CO]]; J. Angle *et al.* [XENON10 Collaboration], Phys. Rev. Lett. **107**, 051301 (2011) [arXiv:1104.3088 [astro-ph.CO]].
- [5] D. S. Akerib *et al.* [CDMS Collaboration], Phys. Rev. D **82**, 122004 (2010) [arXiv:1010.4290 [astro-ph.CO]]; Z. Ahmed *et al.* [CDMS-II Collaboration], Phys. Rev. Lett. **106**, 131302 (2011) [arXiv:1011.2482 [astro-ph.CO]].
- [6] D. S. Akerib *et al.*, Phys. Rev. Lett. **112**, 091303(2014) [arXiv:1310.8214 [astro-ph.CO]].
- [7] M. I. Gresham and K. M. Zurek, Phys. Rev. D **89**, 016017 (2014) [arXiv:1311.2082 [hep-ph]].
- [8] R. Agnese *et al.*, arXiv:1402.7137 [hep-ex].
- [9] W. Zhao *et al.*, arXiv:1404.4946 [hep-ex].
- [10] J. Alwall, P. Demin, S. de Visscher, R. Frederix, M. Herquet, F. Maltoni and T. Plehn *et al.*, JHEP **0709**, 028 (2007) [arXiv:0706.2334 [hep-ph]]; J. Alwall, M. Herquet, F. Maltoni, O. Mattelaer and T. Stelzer, JHEP **1106**, 128 (2011) [arXiv:1106.0522 [hep-ph]].
- [11] T. Sjostrand, S. Mrenna and P. Z. Skands, JHEP **0605**, 026 (2006) [hep-ph/0603175].

- [12] J. Conway et al., PGS (Pretty Good Simulation), <http://physics.ucdavis.edu/~conway/research/software/pgs/pgs4-general.htm>
- [13] P. J. Fox, R. Harnik, J. Kopp and Y. Tsai, Phys. Rev. D **85**, 056011 (2012) [arXiv:1109.4398 [hep-ph]].
- [14] G. Aad *et al.* [ATLAS Collaboration], Phys. Lett. B **705**, 294 (2011) [arXiv:1106.5327 [hep-ex]]; Tech. Rep. ATLAS-CONF-2011-096, CERN, Geneva (2011).
- [15] M. L. Mangano, M. Moretti and R. Pittau, Nucl. Phys. B **632**, 343 (2002) [hep-ph/0108069]; M. L. Mangano, M. Moretti, F. Piccinini and M. Treccani, JHEP **0701**, 013 (2007) [hep-ph/0611129].
- [16] S. Chatrchyan *et al.* [CMS Collaboration], Phys. Rev. Lett. **107**, 201804 (2011) [arXiv:1106.4775 [hep-ex]]; Tech. Rep. CMS-PAS-EXO-11-059, CERN, Geneva (2011).
- [17] V. D. Barger, A. D. Martin and R. J. N. Phillips, Phys. Lett. B **125**, 339 (1983).
- [18] R. W. Brown, K. L. Kowalski and S. J. Brodsky, Phys. Rev. D **28**, 624 (1983).
- [19] CMS Collaboration, CMS-PAS-EXO-12-048 (<http://cds.cern.ch/record/1525585>)
- [20] CMS Collaboration, Phys. Rev. Lett. **108**, 261803 (2012). [arXiv:1204.0821 [hep-ex]].
- [21] ATLAS Collaboration, ATLAS-CONF-2012-147 (<http://cds.cern.ch/record/1493486>)
- [22] KIAS School on MadGraph for LHC Physics Simulation (24-29, October 2011, KIAS, Seoul, <http://workshop.kias.re.kr/MGLP>).